

THESIS

A METHOD USING DRAWDOWN DERIVATIVES TO ESTIMATE AQUIFER PROPERTIES NEAR  
ACTIVE GROUNDWATER PRODUCTION WELL FIELDS

Submitted by

Alan Lewis

Department of Geosciences

In partial fulfillment of the requirements

For the Degree of Master of Science

Colorado State University

Fort Collins, Colorado

Summer, 2014

Masters Committee:

Advisor: Michael Ronayne

Tom Sale

William Sanford

Copyright by Alan Lewis 2014

All Rights Reserved

## ABSTRACT

### A METHOD USING DRAWDOWN DERIVATIVES TO ESTIMATE AQUIFER PROPERTIES NEAR ACTIVE GROUNDWATER PRODUCTION WELL FIELDS

This thesis describes the development of a new inverse modeling approach to estimate aquifer properties in the vicinity of continuously-pumped well fields. The specific emphasis is on deep bedrock aquifers where monitoring well installation is often not practicable due to high drilling costs. In these settings, water levels from groundwater production wells offer a transient dataset that can be used to estimate aquifer properties. Well interference effects, if detectable at neighboring production wells, allow for an interrogated aquifer volume that is larger (and therefore more representative at the well field scale) when compared to single-well hydraulic tests.

The parameter estimation method utilizes drawdown derivatives to estimate the aquifer transmissivity and storativity. The forward model consists of an initial water level (or a recoverable water level drift function), an analytical solution for aquifer drawdown, and a correction term for well loss. The aquifer drawdown component is based on superposition of the Theis solution, although other analytical solutions are also applicable. The observed dataset was judiciously trimmed to reduce computer run-time while retaining enough points to adequately characterize aquifer and well parameters. By limiting observation points to special domains, the calculated drawdown and observed well water level derivatives with respect to time are independent of well loss, and therefore the transmissivity and storativity can be estimated without knowledge of the recoverable water level or loss coefficient for individual pumping wells. Aquifer properties in the forward model were estimated by minimizing the difference between the modeled and observed drawdown derivatives.

The parameter estimation method is tested using hourly water level and pumping data from municipal well fields producing groundwater from sandstone aquifers of the Denver Basin. Data collected over a seven-year period from two distinct well fields, one operating in the Denver aquifer and another operating in the Arapahoe aquifer, are considered. The estimated transmissivities are 30.0 m<sup>2</sup>/d and 46.5 m<sup>2</sup>/d for the Denver and Arapahoe aquifers, respectively, whereas the storativities are  $4.7 \times 10^{-4}$  and  $2.0 \times 10^{-4}$ , respectively. These estimates are within the range of previously reported values, indicating that production well data can be used to derive reasonable aquifer properties. A separate synthetic aquifer test case was considered to further test the parameter estimation methodology, as well as to evaluate the appearance of Theis-like response behavior at the wells. Synthetic water levels were generated using a numerical model with geostatistically-simulated heterogeneity that is characteristic of the Denver Basin (sandstone bodies separated by less permeable inter-bedded siltstone and shale). Analysis of the synthetic water levels revealed meaningful hydraulic properties; the effective hydraulic conductivity (best-fit transmissivity divided by the modeled aquifer thickness) was slightly higher than the geometric mean hydraulic conductivity of the heterogeneous field.

In addition to aquifer properties, observed water level data were used to estimate the well-loss coefficient and recoverable water level for individual pumping wells. Loss coefficients obtained for wells in the Denver Basin indicate that this mechanism (head losses due to turbulence around the well screen) may contribute between 20 and 150 m of the total drawdown (based on a pumping rate of 1500 m<sup>3</sup>/d) commonly observed in these wells. The recoverable water level at each well, when fit with a linear drift function, provides a means of investigating the prevailing trend in aquifer heads due to other regional influences outside the modeled well field.

## ACKNOWLEDGEMENTS

I would like to thank all members of my committee. I am particularly grateful to Dr. Michael Ronayne for accepting me as a graduate student and for investing substantial time in guiding my research and for helping me prepare my thesis. I would also like to thank Dr. Tom Sale for his input and wealth of knowledge about our study area and well field operations. Lastly, I would like to thank Dr. William Sanford for always having a unique perspective on things and making me think in different ways.

I am thankful to everyone who gave me a place to stay while I prepared for graduate school, including Gary and Darlene Smith, Travis and Allison Allen, and Rick and Teresa Dorrity. I would also like to thank Lewis Collard for his computer guidance, Ron Millikan for helping me format my thesis, and Audrey Crockett for her suggestions on improving my defense presentation and in general for always providing a reasoned opinion when I needed one.

I gratefully acknowledge the Town of Castle Rock, CO for providing the data and financial support for this project. Additional support for my research and conference travel was provided by Arcadis-CSU Center for Excellence in Remediation Hydrogeology. I also thank the Department of Geosciences for providing me with funding as a graduate teaching assistant during my first two semesters.

## TABLE OF CONTENTS

ABSTRACT.....	ii
ACKNOWLEDGEMENTS.....	iv
LIST OF TABLES.....	vii
LIST OF FIGURES.....	viii
1 INTRODUCTION.....	1
2 HYDROGEOLOGIC SETTING.....	4
3 METHODS.....	8
3.1 Forward Model.....	8
3.2 Parameter Estimation.....	11
3.3 Corrections.....	15
4 TEST CASES.....	16
4.1 Field Application.....	16
4.1.1 Processing Observation Data.....	17
4.1.2 Results and Discussion.....	19
4.2 Synthetic Well Field.....	28
4.2.1 Model Methodology.....	28
4.2.2 Results and Discussion.....	30
5 CONCLUSIONS AND FUTURE RESEARCH DIRECTIONS.....	34
5.1 Summary and Conclusions.....	34
5.2 Future Research.....	35
REFERENCES.....	37
APPENDIX A: INVERSE SOLUTIONS FOR ALL WELL FIELDS.....	40
A.1 Summary of Estimated Aquifer Properties at All Locations.....	40
A.2 Drift Lines.....	40
A.2.1 Arapahoe.....	40
A.2.1 Denver.....	41
A.2.1 Dawson.....	41
A.3 Well-Loss Coefficients.....	42
A.3.1 Arapahoe.....	42
A.3.1 Denver.....	43
A.3.1 Dawson.....	43
A.4 Model Fit Hydrographs.....	44

A.4.1 Arapahoe .....	44
A.4.2 Denver .....	48
A.4.3 Dawson .....	52
APPENDIX B: PYTHEIS INSTALLATION AND USAGE .....	53
B.1 Software Requirements (Installation Required) .....	53
B.1.1 Python Interpreter .....	53
B.1.2 NumPy, SciPy, and Matplotlib .....	54
B.1.3 PyQt .....	54
B.1.4 Troubleshooting .....	54
B.2 Software Requirements (Pre-Packaged) .....	55
B.2.1 GNU Science Library .....	55
B.2.2 FFmpeg .....	55
B.3 GUI Usage .....	56
B.3.1 Pre-Processing Data .....	56
B.3.2 Creating and Editing Wellfields .....	57
B.3.3 Setting Parsing Options .....	58
B.3.4 Conducting Parameter Estimation .....	60
B.3.5 Creating an Animation .....	63

## LIST OF TABLES

<b>Table 1:</b> Estimated aquifer properties for Denver Basin test cases .....	22
<b>Table 2:</b> Estimated well properties for Denver Basin test cases .....	23
<b>Table 3:</b> Estimated aquifer properties for synthetic test cases.....	32
<b>Table 4:</b> Comparison of the effective hydraulic conductivity (obtained by parameter estimation) to mean K values for the synthetic heterogeneous field. ....	33
<b>Table 5:</b> Comparison of the estimated recoverable water levels to synthetic water levels simulated for each well in the steady-state period prior to pumping. ....	33



## LIST OF FIGURES

<b>Figure 1:</b> West to east geologic cross section for the Denver Basin .....	4
<b>Figure 2:</b> Interpreted geologic cross section in the vicinity of Castle Rock, CO .....	7
<b>Figure 3:</b> Components of drawdown.....	10
<b>Figure 4:</b> Illustration of numerical averaging scheme to approximate the water level (or drawdown) derivative .....	12
<b>Figure 5:</b> Flow chart illustrating the procedure for estimating aquifer and well properties.....	14
<b>Figure 6:</b> Planview maps showing well locations within two Castle Rock well fields used as test cases.	16
<b>Figure 7:</b> Example water level and pumping rate record for a well operating in the Denver aquifer .....	18
<b>Figure 8:</b> Well interference due to pumping in an adjacent well field .....	19
<b>Figure 9:</b> Comparison of modeled and observed water levels for the Castle Oaks well field (Denver aquifer). Constant well-loss coefficient .....	24
<b>Figure 10:</b> Comparison of modeled and observed water levels for the Meadows well field (Arapahoe aquifer). Constant well-loss coefficient .....	25
<b>Figure 11:</b> Comparison of modeled and observed water levels for the Castle Oaks well field (Denver aquifer). Time-varying well loss coefficient.....	27
<b>Figure 12:</b> Synthetic hydraulic conductivity field generated using MPS simulation .....	28
<b>Figure 13:</b> Synthetic well field map .....	29
<b>Figure 14:</b> Simulated water levels and modeled pumping rates for synthetic well field. ....	30
<b>Figure 15:</b> Fit of analytical model to synthetic water level observations after parameter estimation.....	32

## INTRODUCTION

Estimation of aquifer properties in continuously-pumped, municipal well fields is complicated by an inability to cease groundwater production to perform a traditional aquifer test. Fortunately, widespread use of pressure transducers and digital flow recorders has provided large databases of analyzable well pressure and pumping rate records. Recorded fluid pressures at groundwater production wells are influenced by aquifer properties such as transmissivity and storativity, recoverable (non-pumping) water levels, and well condition/health. Quantifying these influences is important and affects decisions made in well field management.

By estimating aquifer transmissivity and well-loss coefficients, well field managers can design more energy-efficient pumping schemes. The energy requirement for pumping is directly proportional to the hydraulic lift [Sterrett, 2007]; maintaining higher water levels in production wells will therefore translate into energy savings. In addition, an accurate estimate of storativity is important for quantifying groundwater availability (e.g., municipal supply wells in Colorado extract over 100 million cubic meters of groundwater per year). However it is difficult to determine the storativity with confidence because it is influenced by estimated transmissivity [Beckie and Harvey, 2002] and measurement location in heterogeneous systems [Meier et al., 1998]. Following the convention of Sánchez-Vila et al. [2006], hydraulic properties derived from model-fitting are herein referred to as “estimated” parameters to acknowledge uncertainty associated with spatial heterogeneity, as well as the dependence of derived values on the interpretation method. “Effective” parameters, in comparison, are based on an ensemble average over many realizations.

The objective of this study is to develop a method for estimating aquifer parameters and well-loss coefficients in a continuously-pumped well field given pumping history and well pressure recordings when static water level is unknown. A forward model using the Theis solution super-positioned in space

and time is used with a simple empirical well-loss function to identify aquifer parameters using observed water level data from groundwater production wells. Previous work by Davis [2013] used a similar forward model to estimate aquifer parameters from active well field data, but was focused strongly on cost analysis of pumping schemes, rather than on developing a robust inverse procedure for estimating aquifer properties. Aquifer and well parameters were fit by visually matching observed to modeled curves, which is time consuming and limits confidence in the final solution.

While literature exists on how heterogeneity influences aquifer drawdown [e.g., Oliver, 1993; Leven and Dietrich, 2006; Tumlinson et al., 2006; Ronayne et al., 2008], there are fewer suggestions or rules of thumb on how to determine when a system should be considered “too heterogeneous” to use a simple model that assumes uniform hydraulic properties. A key aim of this thesis is to determine whether or not useful parameter values may be obtained from continuously-pumped, groundwater production wells. As suggested by Harp and Vesselinov [2011], hydraulic parameters estimated using simplified analytical models may at least provide useful initial guesses for developing more complex heterogeneous models.

Following in the footsteps of Renard et al. [2009] and Bourdet et al. [1989], we make use of the drawdown derivative. In this study, we focus on water level records from pumping wells and show that, in some time domains, the drawdown derivative with respect to time is not a function of static water level or well-loss coefficients, and may be used to estimate aquifer transmissivity and storativity values. The estimated parameters may then be used to subsequently best-fit static water levels and well-loss coefficients. One novel aspect of the proposed method is in breaking one large inverse problem into two smaller ones, thereby reducing calculation time and increasing the likelihood of finding global minimums in the objective function.

The parameter estimation method developed in this study is tested using actual municipal well field data from the Denver Basin aquifer system, as well as synthetic water level datasets generated with a numerical model. The primary goal is to estimate aquifer parameters, but also to develop some

considerations for working with continuously-pumped well field data sets and to highlight the importance of developing methods and models to use in such systems, which are geographically widespread, yet have not been extensively studied.

## HYDROGEOLOGIC SETTING

The Denver Basin aquifer system is a group of confined, deep-bedrock sandstones located east of the Colorado Front Range that spans approximately 320 kilometers (~200 miles) from north to south, where it is bounded by the Greeley and Apishapa arches. The aquifer system is underlain by the Cretaceous Pierre Shale and, in some localities, overlain by an alluvial aquifer that follows major surface water drainages [Paschke et al., 2011].

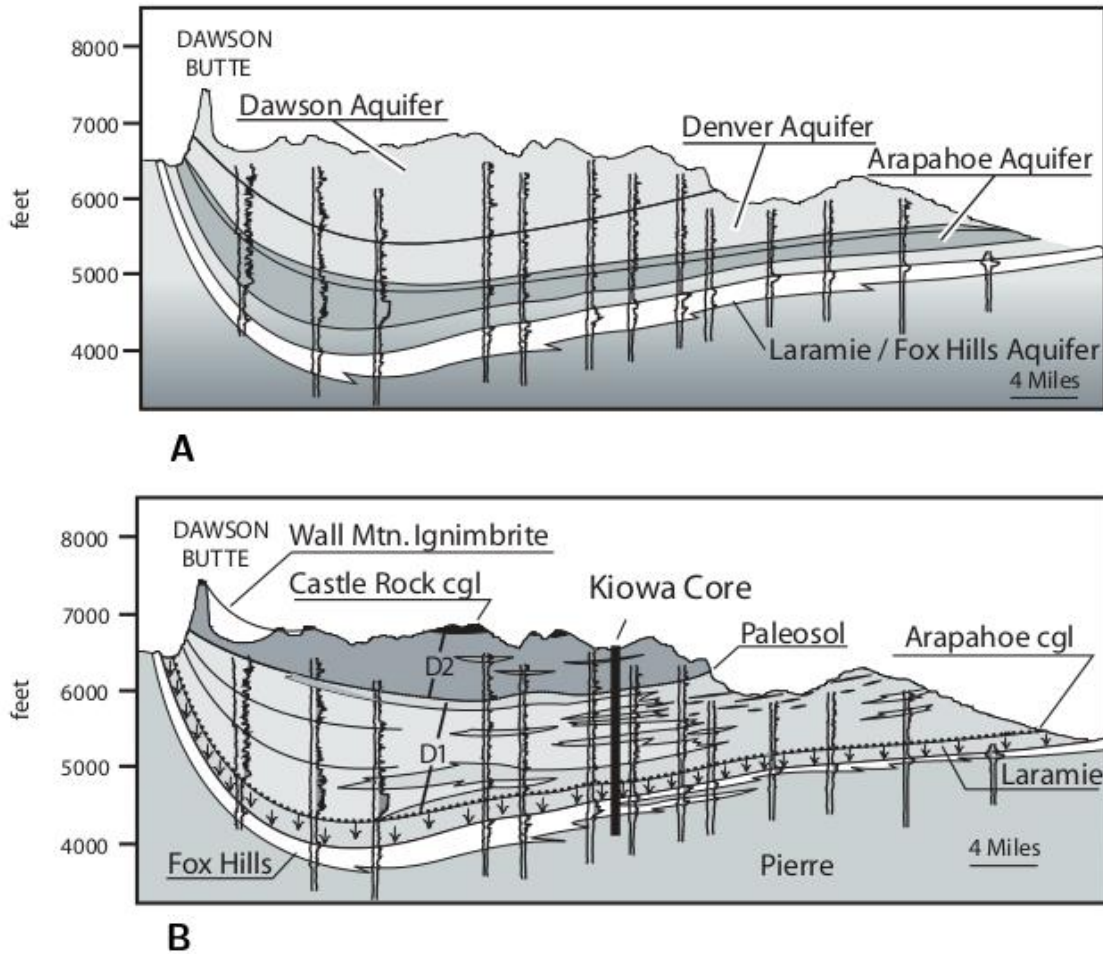


**Figure 1:** West to east geologic cross section for the Denver Basin. (A) Four aquifer classification scheme. (B) Classification scheme proposed by Reynolds [2002]. Figure from Reynolds [2002]

The Denver Basin aquifer system was deposited during the Laramide orogeny during the late-Cretaceous through the Tertiary. The system as a whole can be described structurally as a bowl-shaped, double-plunging syncline [Anderman and Ackman, 1963]. While differences exist between aquifer units, fluvial deposits are characteristic throughout much of the entire system.

Raynolds [2002] has suggested grouping the basin into two large, unconformity-bounded sequences representing two distinct depositional pulses (figure 1). The boundary between the D1 and D2 sequences is thought to be the result of a period of intense weathering and can be difficult to distinguish in cores and outcrops [Raynolds, 2002]. The top of the D1 sequence has been dated at around 63-65 Ma [Mutschler et al., 1987; Obradovich, 2002] and the bottom of the D2 sequence has been dated around 54 Ma [Soister and Tschudy, 1978]. Also illustrated in figure 1 is the four-aquifer classification scheme used by the Office of the State Engineer of Colorado, which involves four primary bedrock aquifers that are separated by confining units. From oldest to youngest, these aquifer units are the Laramie Fox-Hills, Arapahoe, Denver, and Dawson (Table A3, from Paschke et al. [2011]). The four-aquifer conceptualization is used in this thesis (specifically when referring to test application data from the Denver and Arapahoe aquifers) in order to be consistent with other reports and the nomenclature commonly used at our field site. However, we acknowledge that the interpretation of Raynolds [2002] is based on more recent, detailed geologic investigation, and we use this interpretation as well as other local data to guide the development of a synthetic aquifer model.

The Laramie Fox-Hills aquifer formed during regression of the Interior Cretaceous Seaway and uplift of the Front Range. Subsequently, the regression caused formation of a deltaic environment consisting of interbedded clay, coal, and fluvial deposits. The Laramie Fox-Hills aquifer is 0-500 ft thick and is overlain by a 100-700 ft thick confining unit composed largely of shale and coal seams [Robson, 1987]

The Arapahoe aquifer is comprised of alluvial fan deposits from the late Cretaceous. The Arapahoe is a 400-600 ft thick collection of interbedded conglomerate, sandstone, siltstone, and shale overlain by a 0-250 ft thick confining unit [Romero, 1976; Robson, 1987].

The Denver aquifer is a continuation of alluvial fan deposits. Composition is regionally different, with sandstone beds being more prevalent on the western flank and finer-grained sediments and coal being more common in the east [Crifasi, 1992]. The Denver aquifer spans from the late Cretaceous to the Tertiary and is a 600-1200 ft thick sequence of interbedded shale, claystone, siltstone, sandstone, coal, and volcanics [Romero, 1976; Robson, 1987].

The Dawson aquifer is a fluvial deposit consisting of interbedded conglomerate, sandstone, siltstone, and shale [Romero, 1976; Robson, 1987]. The unit ranges from 100 to 1100 ft thick and is overlain by an easily identifiable shale and clay confining unit in the north. The confining unit, when present, is difficult to distinguish in the southern extent. Near Castle Rock, CO, the Dawson aquifer is overlain by the Castle Rock Conglomerate (figure 1b).

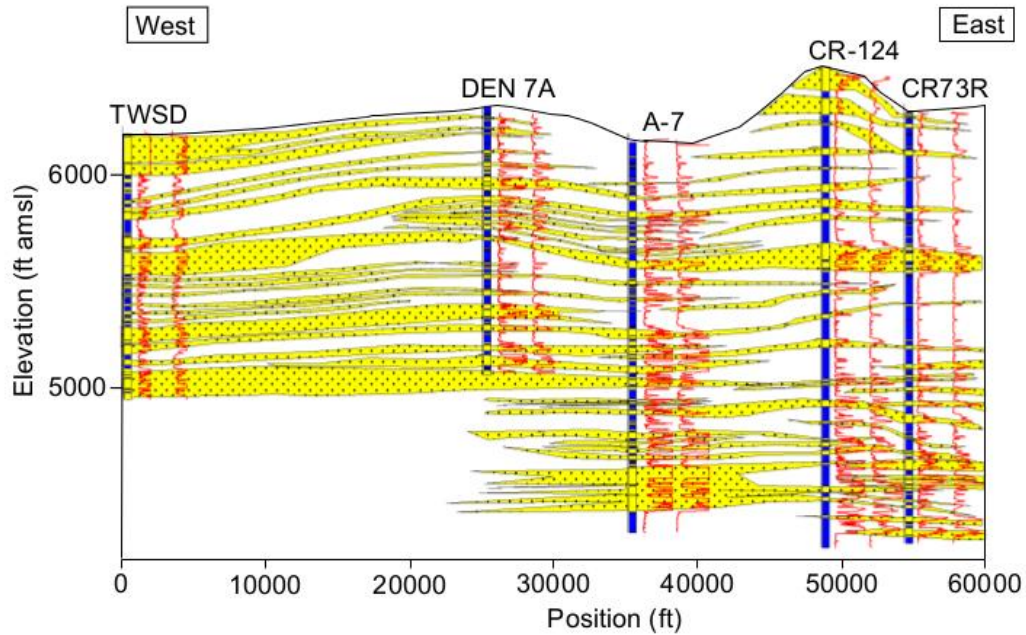


**Figure 2:** Interpreted geologic cross section in the vicinity of Castle Rock, CO based on geophysical logging. Resistivity logs are illustrated as red lines. Interpreted sandstone bodies are shown in yellow. Modified from Sale et al. [2010].

This study focuses on portions of the Denver and Arapahoe aquifers located near the Town of Castle Rock, CO. Sale et al. [2010] utilized core samples and geophysical logging to interpret the aquifer structure in this area (figure 2). They found that proportions and thicknesses of sandstones are highly dependent on location. The intervening material between sandstones (figure 2) consists of silty deposits with substantially lower permeability. Although larger-scale regional trends are important in the Denver Basin aquifer system, this study considers heterogeneity at the well-field scale (100s of meters to several kilometers).



### 3.1 Forward Model

The forward model selected to calculate transient aquifer drawdown assumes radial flow to pumping wells in a homogeneous and isotropic system. With reasonable boundary conditions, the solution to which is (Theis, 1935)

$$s_{aq} = \frac{Q}{4\pi T} W(u) \quad (3.1)$$

$$u = \frac{r^2 S}{4Tt}$$

where  $s_{aq}$  is drawdown due to pumping in the aquifer formation [L],  $Q$  is a constant pumping rate [ $L^3T^{-1}$ ],  $T$  is transmissivity [ $L^2T^{-1}$ ],  $r$  is the radial distance from a pumping location [L],  $S$  is storativity,  $t$  is time [T] since pumping began, and  $W$  is the  $E_1$  exponential integral, commonly referred to as the well function and defined as

$$E_1(u) = \int_u^\infty \frac{e^{-x}}{x} dx$$

Since the governing PDE is linear, the solution in equation (3.1) may be superpositioned in the following way

$$s_{aq} = \sum_{i=1}^m \left\{ \frac{Q_{i,0}}{4\pi T} W(u_{i,0}) + \sum_{j=1}^n \frac{\Delta Q_{i,j}}{4\pi T} W(u_{i,j}) \right\} \quad (3.2)$$

$$u_{i,j} = \frac{r_i S}{4T(t_{i,j} - t)}$$

where  $m$  is the number of pumping wells,  $n$  is the number of pumping rate changes occurring before time  $t$ , and  $Q_{i,0}$  is the initial pumping rate at time  $t_{i,0}$ . In this study, drawdown is calculated at individual well locations in an active well field. Thus,  $r_i$  may be the radial distance between two production wells or, for the purpose of computing the component of a well's drawdown that is caused by pumping at the same well,  $r_i$  is a short distance that represents the radius of the well bore.

Along with drawdown in the aquifer formation, additional head losses can occur at pumping wells [Jacob, 1947; Ramey, 1982; Konikow et al., 2009]. One commonly used expression for the drawdown due to well-loss effects ( $s_w$ ) can be found in Rorabaugh (1953)

$$s_w = BQ + CQ^n \quad (3.3)$$

which represents head loss due to both laminar ( $BQ$ ) and turbulent ( $CQ^n$ ) flow through a well screen. This study uses a simplified form [Domenico and Schwartz, 1990] which only considers the turbulent well loss and assigns a value of 2 to  $n$ .

$$s_w = CQ^2 \quad (3.4)$$

At low discharge rates, turbulent flow is negligible, and the well loss is dominated by laminar flow. In our model, pumping rates are assumed to be high enough that turbulent well loss is always present. Total drawdown (figure 3) is calculated from the combined effects of equations (3.2) and (3.4)

$$s_{total} = s_{aq} + s_w \quad (3.5)$$

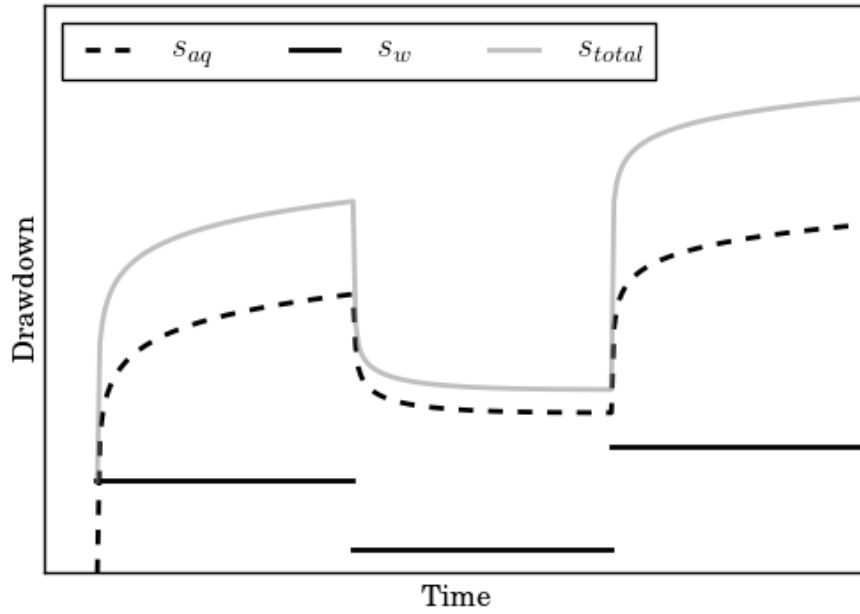


**Figure 3:** Components of drawdown. Total drawdown ( $s_{total}$ ) is due to the combined effects of drawdown in the aquifer ( $s_{aq}$ ) and drawdown due to well loss ( $s_w$ ).

The water level within a production well ( $h_{well}$ ) is a composite hydraulic head (influenced by the variable heads at different depth intervals along the well screen) that may be approximated as

$$h_{well} = h_0 - s_{aq} - s_w \quad (3.6)$$

where  $h_{well}$  is water level within a production well and  $h_0$  is a recoverable water level (i.e., the level to which the water level in a well would eventually recover if pumping was stopped). In the aquifer testing literature,  $h_0$  is conceptualized as the static water level, or the hydraulic head prior to the start of

pumping. Because our analysis focuses on continuously pumped well fields where it is difficult to define a meaningful static condition, we utilize the "recoverable" level in the above definition. Further, we note that this level could be represented as a constant or dynamic function (e.g., a drift function to account for temporal trends associated with neighboring pumping, outside the modeled well field, or leakage through confining units).

### 3.2 Parameter Estimation

As indicated in the previous section, water level in a production well depends on the following: the aquifer transmissivity and storativity, a well-loss coefficient, and a recoverable water level. An inverse methodology was developed to estimate these parameter values from the measured time-series data (pumping rates and water levels at individual production wells).

The first step in the procedure is estimation of  $T$  and  $S$ . To obtain a function that is independent of  $C$  and  $h_0$ , which are generally unknown for continuously pumped wells, we differentiate equation (3.6) with respect to time:

$$\frac{\partial}{\partial t} h_{well} = \frac{\partial}{\partial t} (h_0 - s_{aq} - s_w) \quad (3.7)$$

For periods when  $dQ/dt = 0$ , we assume

$$\frac{\partial h_0}{\partial t} = 0; \quad \frac{\partial s_w}{\partial t} = 0 \quad (3.8)$$

which results in the following simplification

$$\frac{\partial h_{well}}{\partial t} = -\frac{\partial s_{aq}}{\partial t} \quad (3.9)$$

indicating that, for a time period when the pumping rate is not changing, the temporal rate of change in the well water level should be equal to  $-\frac{\partial s_{aq}}{\partial t}$  (minus the drawdown derivative for the aquifer).

Equation (3.9) is the basis for estimating  $T$  and  $S$ . We calculate  $-\frac{\partial s_{aq}}{\partial t}$  from computed drawdowns obtained with the forward model described in Section 3.1.  $T$  and  $S$  are adjusted until there is an acceptable match between the observed and modeled derivatives.

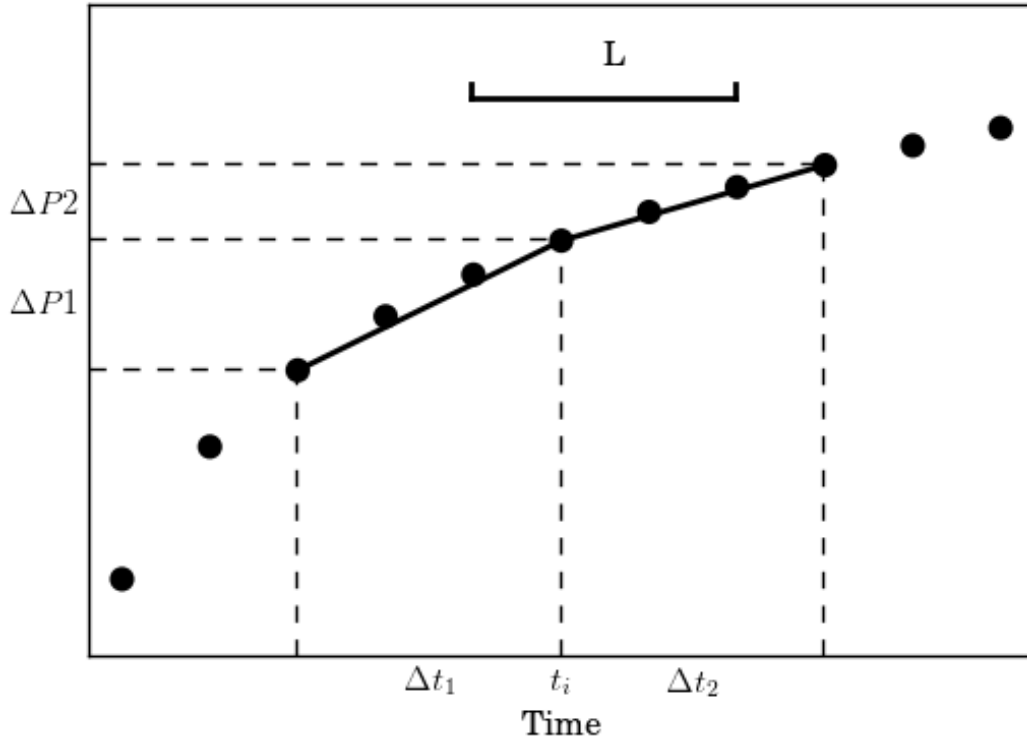


**Figure 4:** Illustration of numerical averaging scheme to approximate the water level (or drawdown) derivative at time  $t = t_i$ . Figure adapted from Bourdet et al. [1989].

One practical challenge for this procedure is the determination of  $\frac{\partial h_{well}}{\partial t}$ . The temporal derivative of observed water level data is characteristically noisy. An algorithm is borrowed from Bourdet et al. [1989] whereby neighboring points are used to calculate an averaged derivative over some length  $L$  (figure 4).  $P$  is used as a generic representation of either observed water level or modeled drawdown.

$$\left(\frac{dP}{dt}\right)_i = \frac{\frac{\Delta P_1}{\Delta t_1} \Delta t_2 + \frac{\Delta P_2}{\Delta t_2} \Delta t_1}{\Delta t_1 + \Delta t_2} \quad (3.10)$$

For well fields instrumented with an automated data acquisition system, water levels are usually recorded at equally spaced intervals ( $\Delta t_1 = \Delta t_2$ ). Taking advantage of this, one may reduce equation (3.10) to

$$\left(\frac{dP}{dt}\right)_i = \frac{\Delta P_1 + \Delta P_2}{2\Delta t} = \frac{\Delta P_{avg}}{\Delta t} \quad (3.11)$$

The Levenberg-Marquardt algorithm [Marquardt, 1963] is used to identify values of  $T$  and  $S$  that minimize the difference between the observed and modeled derivative. Cooley [1985] defends usage of the LM algorithm based on its relatively high accuracy per runtime. Estimates are sought that minimize the objective function

$$\sum_{i=1}^m \sum_{j=1}^{nd} \left[ \left( \frac{\partial h_{well}}{\partial t} \right) + \left( \frac{\partial s_{aq}}{\partial t} \right) \right]_{i,j}^2 \quad (3.12)$$

where  $m$  is the number of wells in a well field and  $nd$  is the number of times when a derivative is approximated using the observed and modeled water levels.

In addition to the aquifer properties, we use the analytical model presented in Section 3.1 to estimate values of  $C$  and  $h_0$  sequentially at each well. During recovery periods ( $Q = 0$ ), we assume  $s_w$  is 0 (equation 3.4) and equation (3.6) reduces to

$$h_{well} = h_0 - s_{aq} \quad (3.13)$$

The objective function (3.14) is applied over  $n$  available points during recovery periods only, when there are negligible well loss effects.

$$\sum_{j=1}^n (h_0 - s_{aq} - h_{well})_j^2 \quad (3.14)$$

Since  $h_{well,i}$  is known from well level records and  $s_{aq,i}$  is previously estimated by minimizing the objective function (3.12),  $h_{0,i}$  is the only unknown.  $h_{0,i}$  is either represented as a static water level or a linear drift function.

Lastly,  $C$  is estimated by minimizing the following objective function using all available data

$$\sum_{j=1}^n (h_0 - s_{aq} - s_w - h_{well})_j^2 \quad (3.15)$$

where  $s_w$  is the only remaining unknown. The complete parameter estimation process is summarized in figure 5.

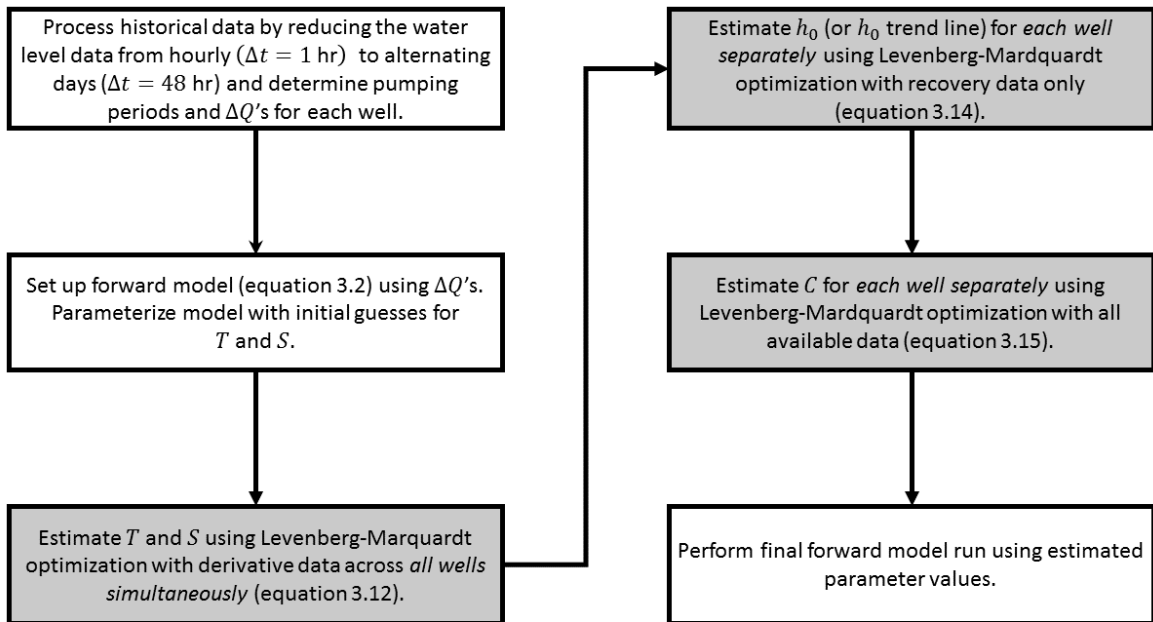


**Figure 5:** Flow chart illustrating the procedure to estimate aquifer and well parameters. Shaded boxes represent the key steps of parameter estimation.

### 3.3 Corrections

In continuously-pumped well fields, pumping may predate the availability of detailed flow rate and water level records. We modeled a spin-up period that was twice as long as the period of observed data at each well and did not consider water level elevations in our objective functions for the first 6 months after pumping records were available. Sensitivity analyses showed that 6 months was a reasonable minimum spin-up period in our model. Drawdown due to past pumping rates becomes less significant as time goes on, but effects do not go away. Also, recoverable water levels are not necessarily static over long periods of time. We found that using a linear drift function rather than a static recoverable water level at each well provided a meaningful correction for predicting water levels.

Also, extended periods of time, it may not be appropriate to assume that the well-loss coefficient is a constant value. Well condition may deteriorate over time due to clogging by sediment or chemical precipitates. When appropriate, we modeled the well-loss coefficient as a linear function of time.

The slope of the drift line and well-loss coefficient function are considered small enough that periods of time over which pumping is constant do not result in a significant change in either the recoverable water level or well loss. Consequently, the simplification made in equation (3.7) still holds.



## TEST CASES

## 4.1 Field Application

The town of Castle rock has four well fields, all of which have wells screened in the Denver and Arapahoe formations. Herein, two sets of wells are addressed: the Castle Oaks that produces groundwater from the Denver aquifer and the Meadows well field that produces groundwater from the Arapahoe aquifer. The spatial distribution of wells is illustrated in Figure 6. The Castle Oaks well field contained 5 pumping wells, and the Meadows well field contained 11 wells. Well head elevations ranged from 1935 to 2010 meters above mean sea level (m amsl) in the Castle Oaks well field and from 1840 to 1910 m above mean sea level in the Meadows well field. Probe depths in these two fields ranged from 410 to 525 m and 460 to 540 m, respectively. Well fields are approximately 2 to 5 kilometers apart, though individual wells on the outer rim of adjacent fields may be separated by as little as 1-2 kilometers.

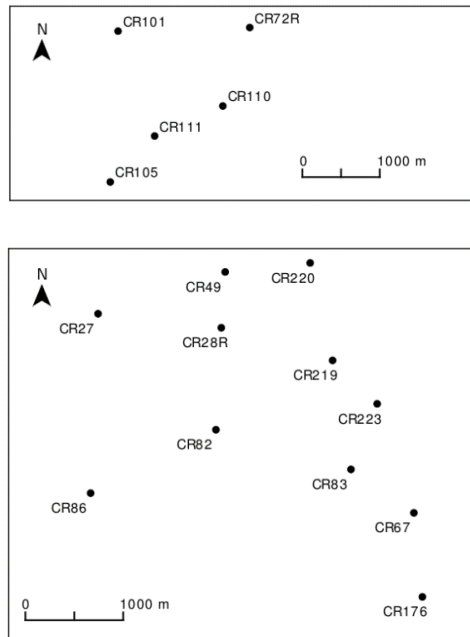


**Figure 6:** Planview maps showing well locations within two Castle Rock well fields used as test cases. (a) Castle Oaks well field in the Denver aquifer. (b) Meadows well field in the Arapahoe aquifer.

#### 4.1.1 Processing Observation Data

Well field data consisted of hourly water levels and pumping rates for each production well over a period of several years (see example time-series data in figure 7). Operational pumping rates are typically between 500 and 3500 m<sup>3</sup>/d. The range of water levels at individual wells can be greater than 150 m.

In addition to the effects of neighboring wells, our forward model calculates drawdown at a production well due to pumping at the same well. An effective well radius ( $r_w$ ) of 0.305 m (1 ft) was chosen based on borehole sizes.

Parameter estimation was performed using manually selected periods of time where pumping rates were constant and drawdown or recovery curves had smooth behavior (i.e., the objective function compared modeled and observed values during these time periods). Noise in observed well level data can be exacerbated in the observed well water level derivative. Recovery periods were favored during estimation of  $S$  and  $T$  because they tended to have smoother behavior (figure 7) and are less likely to be significantly impacted by well inefficiency (equation 3.4).

Water level or pumping rate recordings that were suspected to be erroneous were removed. Noisy level measurements due to small variations in pumping rates not recorded were retained, but not considered in the first step of the inversion process to estimate  $S$  and  $T$ .

Equation (3.4) produces a jump discontinuity in the drawdown due to well loss when there is a change in the pumping rate. In reality, well water levels have a short transition period when adjusting to well loss from two different pumping rates. Water levels collected during the short period of time (one to two days) immediately following changes in pumping rate were excluded from the parameter estimation process to allow well loss to stabilize.

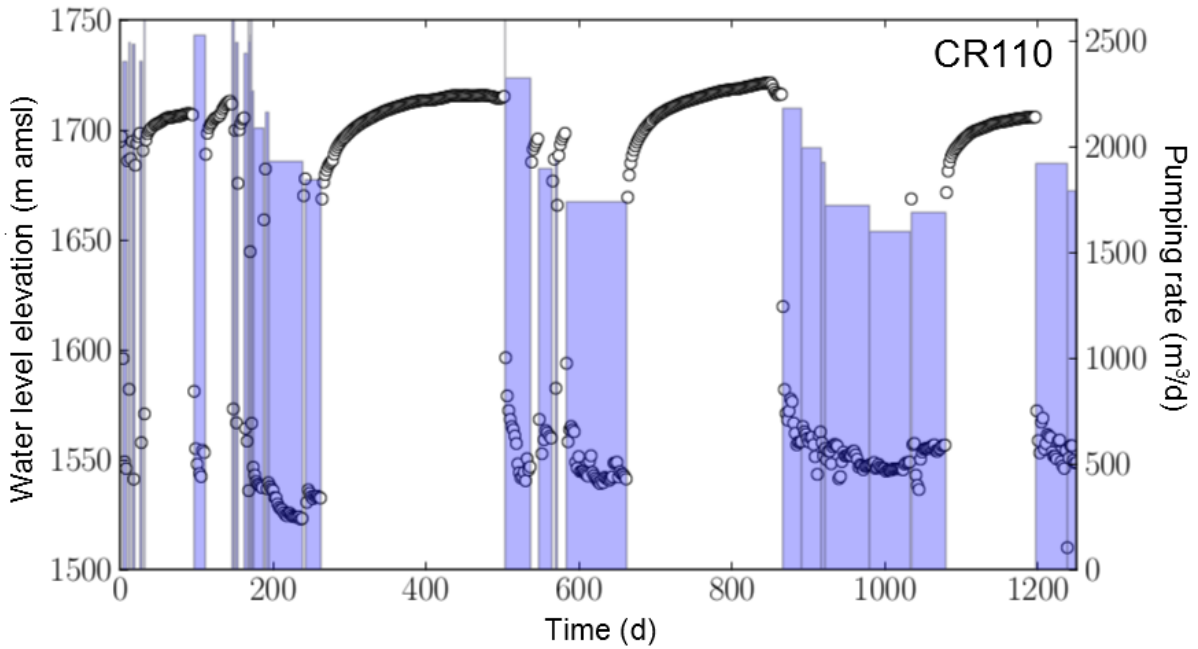


**Figure 7:** Example water level (open circles) and pumping rate (shaded bars) record for well CR110 operating in the Denver aquifer. Hourly data is shown reduced to alternating days ( $\Delta t = 48$  hrs)

When data are collected at a high frequency, the derivative is characteristically noisy. Reducing water level data to daily or alternating days reduced run-time and noise in the derivative. The interval between water level readings ( $\Delta t$ ) must be long enough to avoid excessive noise and short enough to characterize the shape of the drawdown and recovery curves. For the field applications presented in this chapter, a  $\Delta t$  of 48 hours was found to be sufficient.

The number of pumping rates in the original dataset was computationally overwhelming to work with. Two schemes were tested for reducing the number of pumping rates considered. Prior to testing both schemes, all pumping rates less than some threshold  $Q_{min}$  were set to 0 (i.e., when  $Q \leq Q_{min}$ , the pump would be considered off). Our first scheme involved averaging pumping rates over blocks of time that were separated when two adjacent pump rates had a difference of some threshold  $\Delta Q$ . A  $\Delta Q$  of 10 gpm was used for this study. Our second scheme averaged all pumping rates over the entire duration that a well was active, regardless of possible significant changes in pumping rates. Both methods produced similar results for the Denver Basin datasets, but we found that the latter method would occasionally omit

features due to pumping rate changes in the modeled drawdown that are clearly present in the observed data. Thus, the scheme using the threshold  $\Delta Q$  was used for all modeling scenarios included in this thesis.

Changes in the well loss coefficient are known to occur due to well degradation [Sterrett, 2007]. A second parameter estimation was performed in the Denver aquifer well field whereby well efficiency was represented as a linearly increasing function through time. That is, the well loss function was modeled as  $C(t)Q^2$ , where  $C(t) = mt + b$ . A linear well loss term may be too simple, but it serves as a reasonable starting place.

In municipal well fields, wells are pumped at fairly regular pumping rates and it would be uncommon for a well to be pumped at low discharge rates for short durations following a long period of constant, higher discharge. Interference from pumping at adjacent wells can be seen during recovery periods when the slope oscillates from negative to positive. In the Castle Oaks well field, it was necessary to consider pumping from an adjacent Denver aquifer well field to accurately model these interference effects (figure 8).

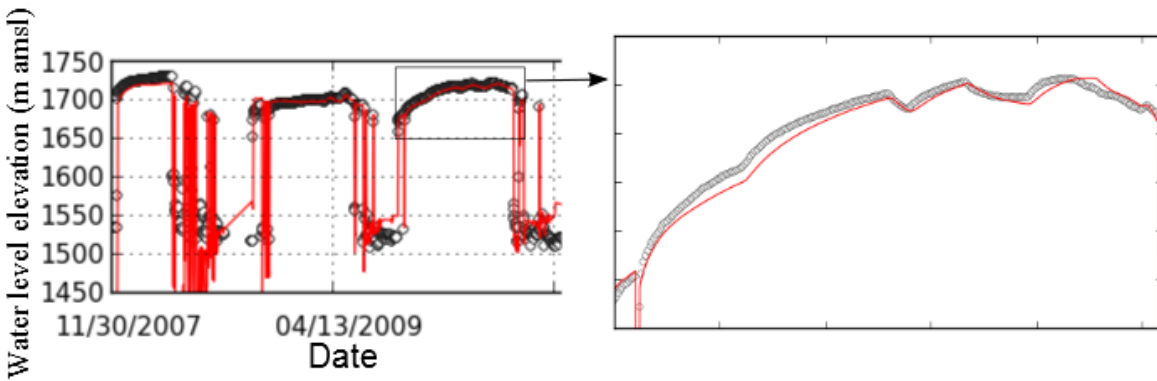


**Figure 8:** Well interference at well CR105 (Castle Oaks, Denver) due to pumping in an adjacent well field. Open circles show the observed water levels; solid line is the model solution.

#### 4.1.2 Results and Discussion

Model results using the estimated transmissivity and storativity for each well field are provided in figures 9 and 10. The Theis superposition model with a linear drift function for recoverable water level

provides an excellent match to observed water levels during recovery periods, when the well is off. During active pumping periods when the water level is low and characterized by greater volatility from day to day, the residuals are higher.

Table 1 summarizes estimated aquifer properties for Denver and Arapahoe test well fields. Transmissivity and storativity estimates are within previously measured ranges. Paschke et al. [2011] report hydraulic conductivities for the Denver aquifer ranging from 0.009 to 7.3 m/d, with a geometric mean of 0.04 m/d. For the Arapahoe aquifer, their reported range is between 0.018 to 3.0 m/d with geometric mean of 0.15 m/d. Assuming aquifer thickness in ranges reported by Paschke et al. [2011], our estimated transmissivities translate to hydraulic conductivities of 0.02 to 0.05 m/d for the Denver aquifer and 0.08 to 0.12 m/d for the Arapahoe aquifer. Transmissivity estimates from single-well recovery tests performed by Hemenway Groundwater Engineering at the Castle Rock wells, are also available for comparison in Davis [2013]. The estimated transmissivities in the Denver aquifer ranged from 26 to 55 m<sup>2</sup>/d and from 25 to 68 m<sup>2</sup>/d in the Arapahoe, which are also consistent with the values we obtained.

Although still within published ranges, our estimated storativities are likely more uncertain than the transmissivity values due to imprecise knowledge of the effective well radii ( $r_w$ ) and skin effects (gravel pack and formation damage). These factors, which are known to influence the storativity derived from single-well aquifer tests [Jacob, 1947], are assumed to also be sources of error in our storativity estimate, given that we use observed water level data at pumping wells. Our parameter estimation is complicated by simultaneously evaluating the combined effects of pumping at each well on other wells and pumping at each well on itself. It might be reasonable to assume that  $r_w$  is at least approximately equal at every well in a well field if they all have the same casing radius, gravel pack, and completion. This being the case, the error in estimated storativity might possibly be attenuated by fitting a single  $r_w$  across all wells simultaneously with storativity and transmissivity, which is an improvement over single well pumping tests where  $r_w$  (and consequently storativity) are uncertain.

Table 2 presents recoverable water levels, drift line slopes, and well-loss coefficients. Note that the recoverable water levels reported in the table actually represent the intercept of the drift line at the beginning of the historical observation period (Nov 30, 2007 for both well fields). While drift line slopes may be interpreted physically as (among other things) pumping at distant well fields, leakage, or recharge, we have no uniquely apparent explanation. Nevertheless, a linear drift is still useful for predicting water level elevations in wells. Drift lines fit with less data over shorter periods of time are less effective at characterizing long-term trends. The effect of small datasets on estimating long-term drift line behavior can be witnessed from the recoverable water levels ( $t_0$  intercepts) reported in Table 2 for wells CR101 and CR72R. These wells have datasets that are temporally displaced from  $t_0$  more than wells CR105, CR110, and CR111 (figure 9) and therefore are less likely to provide a reliable estimate of recoverable water level at that time.

The estimated drift line parameters are also sensitive to modeled pumping history (spin-up period prior to the first time that detailed pumping records are available). We found that adding more synthetic pumping history resulted in drift line slopes that were increasingly negative. The drift lines in table 2 are the result of adding ten years of synthetic pumping history to our models.

Estimates of well-loss coefficient for Denver aquifer wells were consistent with one another and of reasonable magnitude. The median well loss ( $1.4 \times 10^{-5} \text{ d}^2/\text{m}^5$ ) in our Denver aquifer well field represents  $\sim 40 \text{ m}$  of additional drawdown at common pumping rates.

Estimates of well-loss coefficient for Arapahoe wells are also presented in table 2. Our inverse method was constrained to  $C \geq 0$ ; values of 0 indicate that the optimization algorithm attempted to identify a negative well-loss coefficient. Negative well-loss coefficients might result from several factors not captured in our forward model, including local heterogeneity or leakage between aquifers. The Denver and Arapahoe aquifers are known to have similar hydrogeology and negative well-loss coefficients do not show up with the same regularity in Denver aquifer well fields. Leakage from the Denver to the Arapahoe aquifer has been reported elsewhere [e.g., Paschke et al., 2011]; this extra source

of water (which is not accounted for in our model) would explain the tendency of the optimization routine to move toward a negative  $C$  value.

Denver aquifer wells characteristically have increasing error through time during pumping periods and a temporally varying  $C$  value provides a much better match during pumping periods (figure 11). It is unlikely that a simple linear function can accurately characterize the complex mechanisms involved in well degradation, and there is an inevitability of physically unrealistic long-term behavior. However, over the domain of our Denver aquifer model, a linearly increasing well loss function appeared to provide a reasonable correction.

In addition to a temporal trend, other improvements in modeling the well loss effect may be achievable. For example, equation (3.4) assumes a constant radius marking the transition between laminar and turbulent well loss effects. At higher pumping rates, turbulent effects occur at a larger radius from a well, and the exponent  $n$  needs to be larger. Non-zero pumping rates in our well fields tend to be of approximately the same magnitude at individual wells, but vary between wells. A more appropriate well loss function might assign both an exponent ( $n$ ) and well-loss coefficient ( $C$ ) at each well. Assuming that pumping rate magnitudes at all wells in a field are approximately equal, a simple improvement would allow a single  $n$  to be estimated across all wells.

**Table 1:** Estimated aquifer properties for Denver Basin test cases

<b>Aquifer</b>	<b>Storativity</b>	<b>Transmissivity (m<sup>2</sup>/d)</b>
Denver	$4.7 \times 10^{-4}$	30.0
Arapahoe	$2.0 \times 10^{-4}$	46.5

**Table 2:** Estimated well properties for Denver Basin test cases

<b>Well</b>	<b>Recoverable Water Level (m)</b>	<b>Drift Line Slope (m/yr)</b>	<b>Well-Loss Coefficient (d<sup>2</sup>/m<sup>5</sup>)</b>
Denver Wells			
CR72R	1736	-1.4	$2.5 \times 10^{-5}$
CR101	1846	-8.8	$7.6 \times 10^{-6}$
CR105	1779	2.0	$6.8 \times 10^{-5}$
CR110	1786	-1.5	$1.4 \times 10^{-5}$
CR111	1779	-3.2	$1.2 \times 10^{-5}$
Arapahoe Wells			
CR27	1516	-4.5	0
CR28R	1518	-3.1	0
CR49	1513	-0.8	0
CR67	1557	-6.6	0
CR82	1522	0.2	$2.6 \times 10^{-6}$
CR83	1532	-2.7	$1.9 \times 10^{-5}$
CR86	1549	-2.9	$1.0 \times 10^{-4}$
CR176	1547	-0.8	0
CR219	1531	-3.6	0
CR220	1517	-2.2	0
CR223	1533	-3.4	$7.7 \times 10^{-7}$



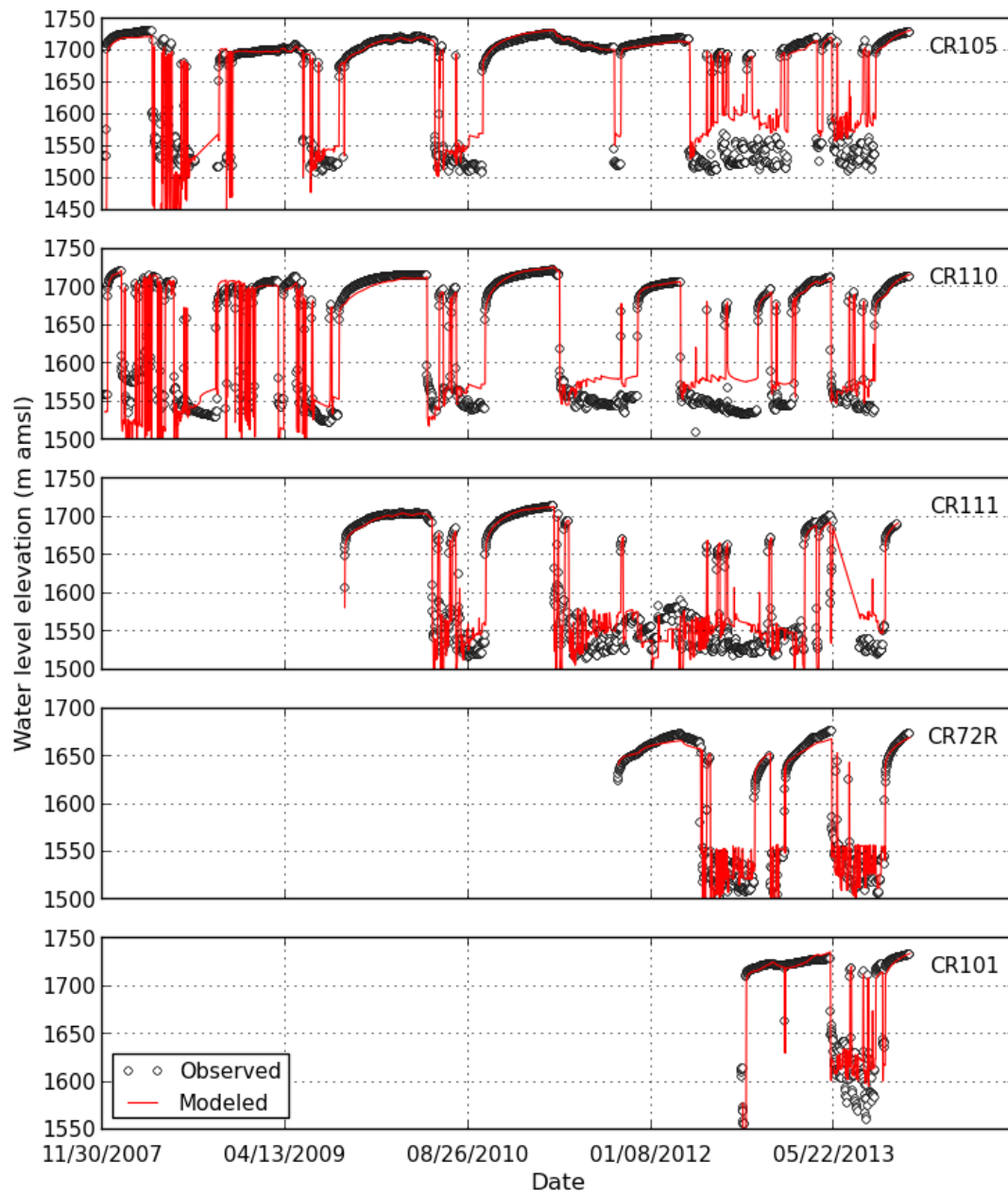


**Figure 9:** Comparison of modeled and observed water levels for the Castle Oaks well field (Denver aquifer). Loss coefficient (C value) for each well is constant through time.

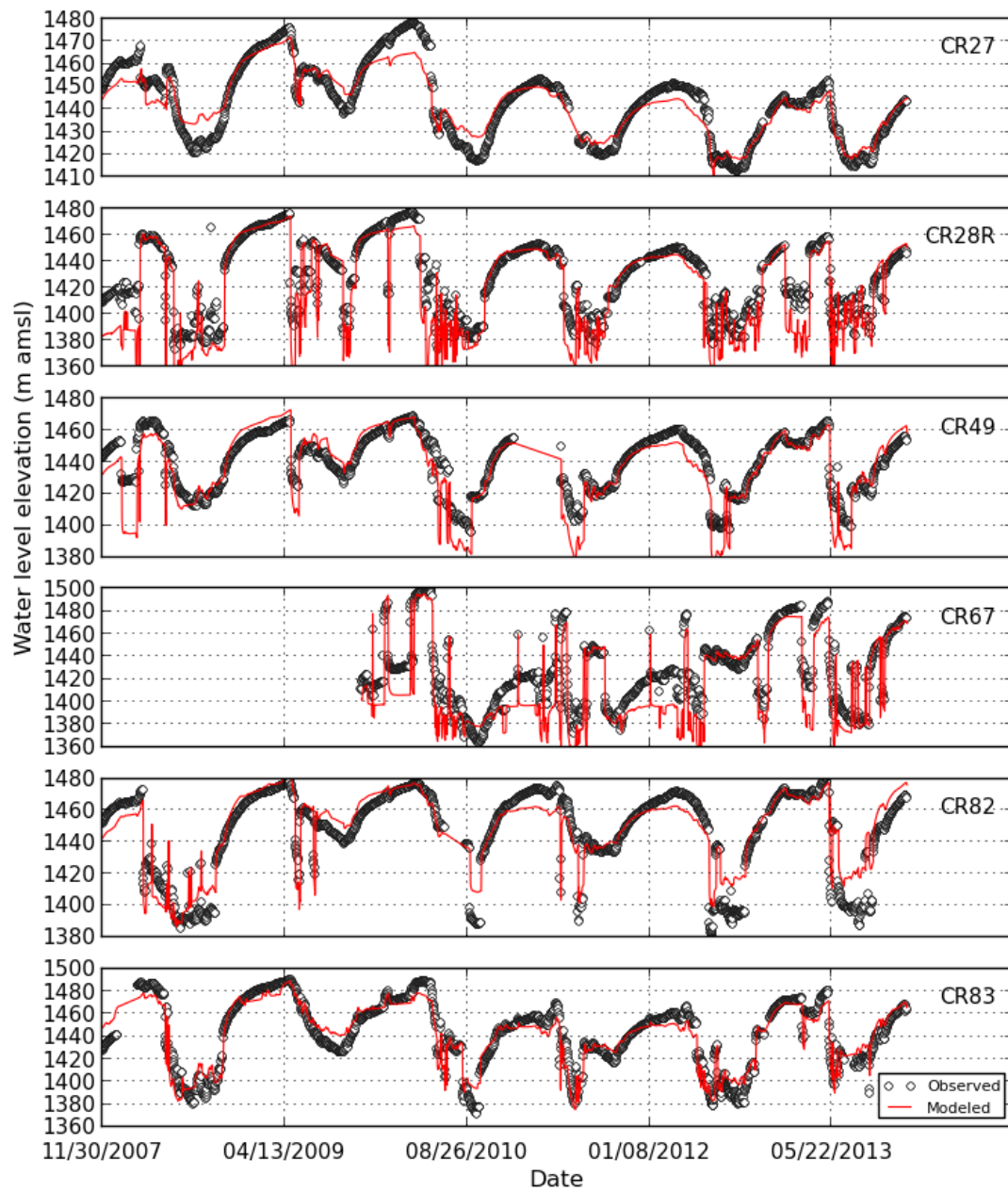


**Figure 10:** Comparison of modeled and observed water levels for the Meadows well field (Arapahoe aquifer). Loss coefficient (C value) for each well is constant through time.

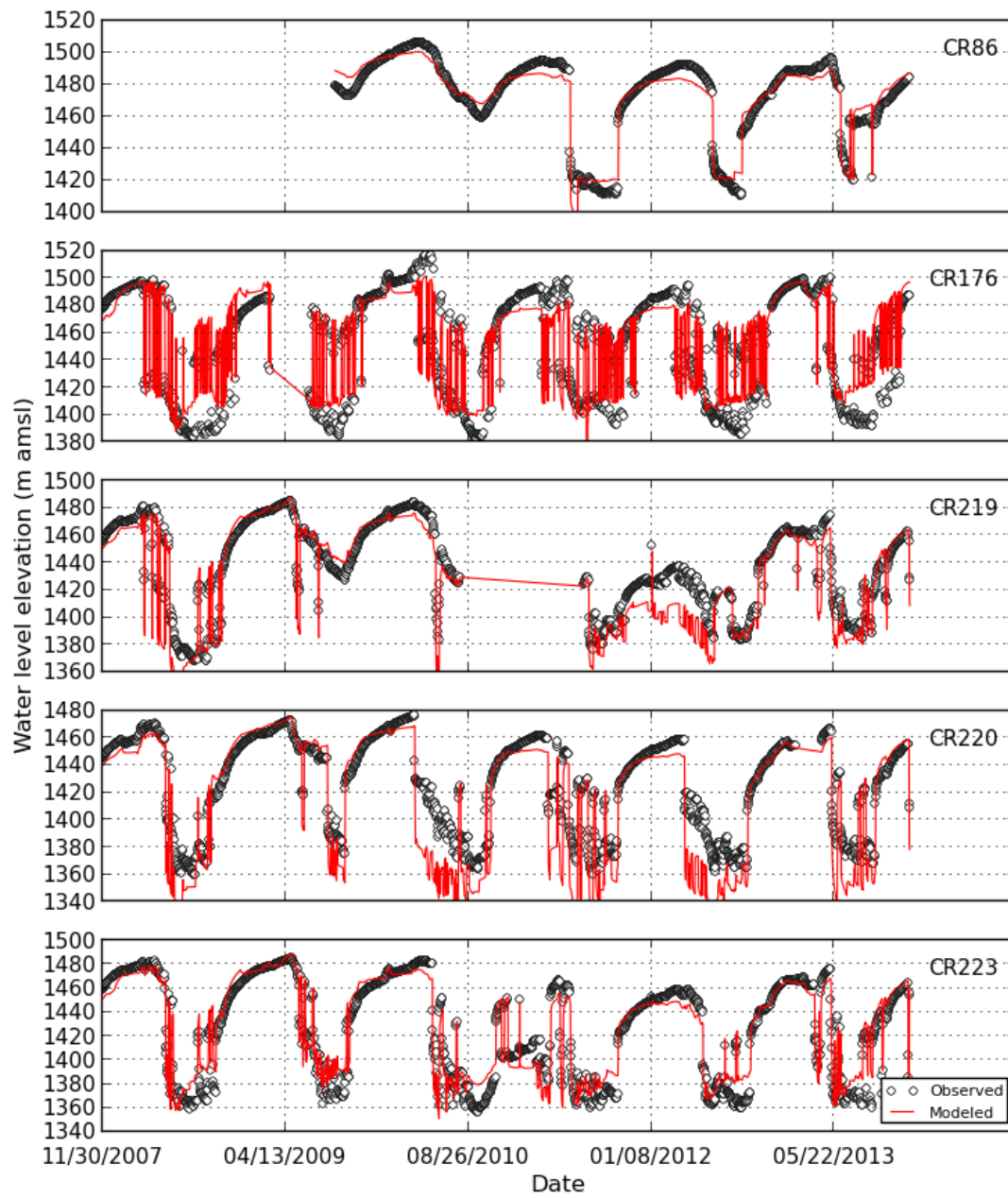
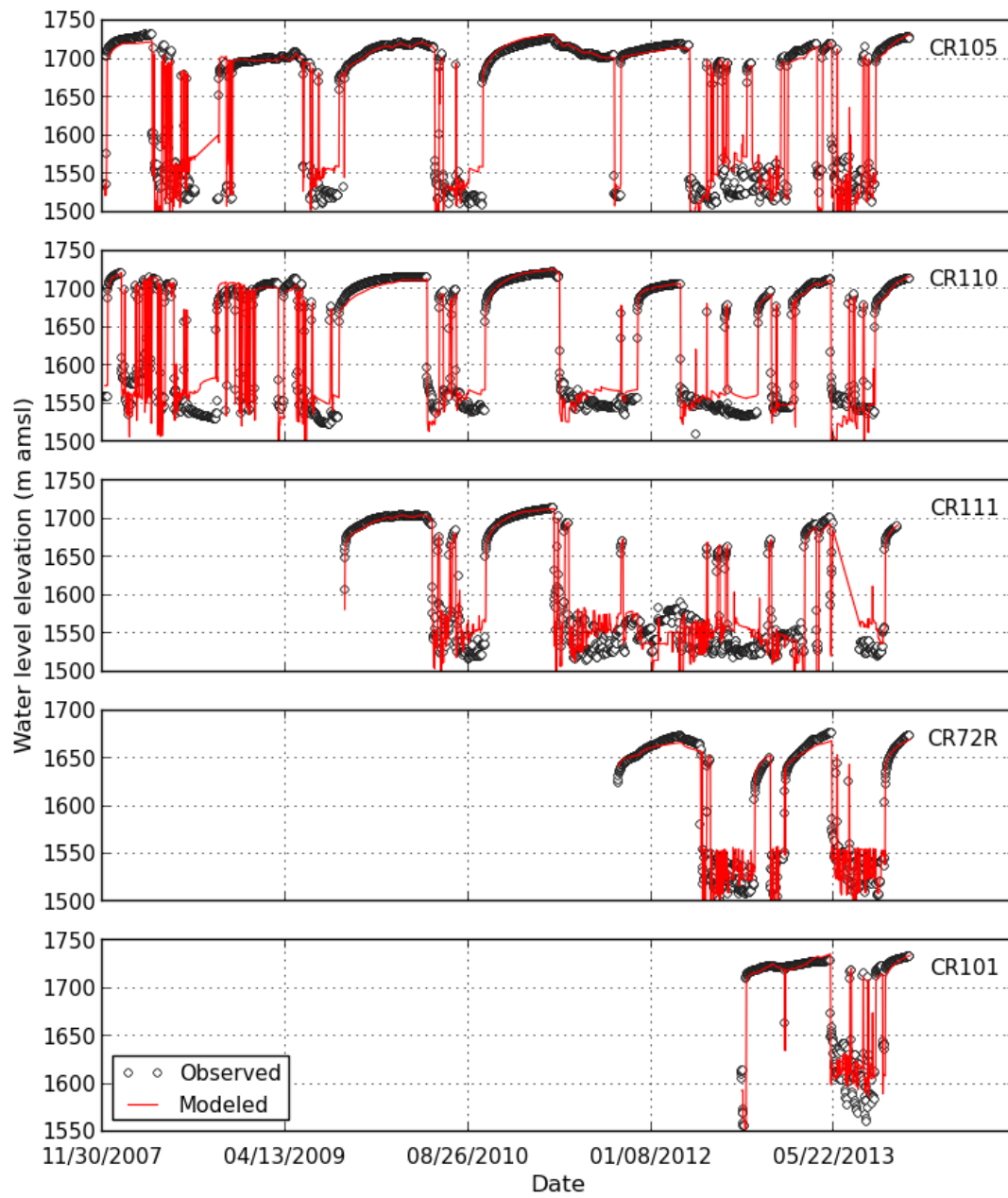


Figure 10 (continued)



**Figure 11:** Comparison of modeled and observed water levels for the Castle Oaks well field (Denver aquifer). Loss coefficient (C value) for each well is time-varying (linear function).

## 4.2 Synthetic Well Field

### 4.2.1 Model Methodology

A three-dimensional (300x300x100), synthetic hydraulic conductivity field (figure 12) was generated using the multiple-point statistical (MPS) algorithm *Impala* [Straubhaar et al., 2011] and *s2Dcd* [Comunian et al., 2012], which extends the capability of *Impala* to include generating three-dimensional MPS models from two-dimensional training images. A portion of figure 2 was used as the training image for this geostatistical simulation. The grid spacing for the simulated field is as follows:  $\Delta x = 27.69$  m;  $\Delta y = 27.69$  m;  $\Delta z = 1.1$  m. Two isotropic hydraulic conductivities (0.1 m/d, 0.005 m/d) were selected to represent differences between the sandstone and silty deposits that occur in the Denver Basin.

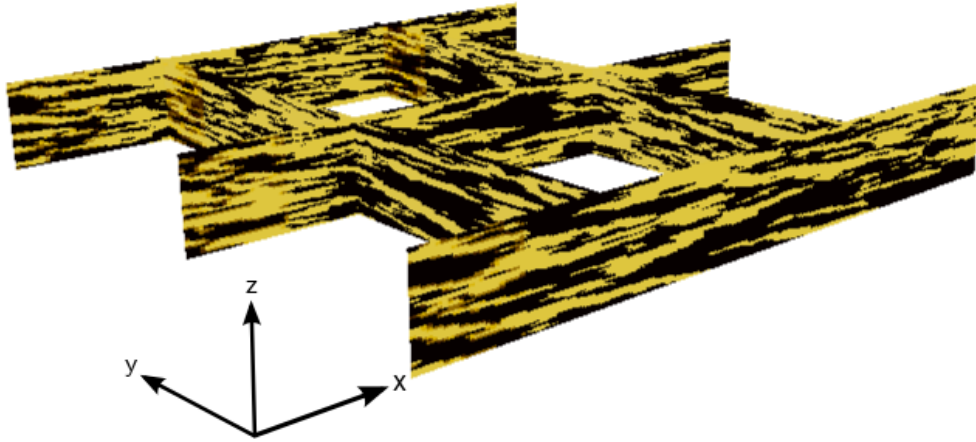


**Figure 12:** Synthetic hydraulic conductivity field generated using MPS simulation. Yellow represents sandstones and black represents siltstones or clays. Model dimensions are approximately 8000 m in the x and y directions, and 110 m in the z direction. 10x vertical exaggeration.

The hydraulic conductivity field was imported into MODFLOW and three synthetic wells (figure 13) were modeled using the multi-node well (MNW2) package [Konikow et al., 2009]. The pumping rates/schedule (figure 14) are characteristic of what one may find at a municipal well field and are implemented using 12 stress periods over a duration of six months. All three wells penetrate the entire thickness of the synthetic aquifer (110 m), which is modeled as a confined system

Our synthetic observation dataset has been simplified by not modeling well loss and the background trend in recoverable water level. The parameter estimation algorithm was modified to find a single recoverable water level (i.e., drift line with zero slope) and no well loss. The MNW2 package uses an approximation based on the steady-state Thiem equation to estimate water levels at well locations within a cell. This approximation, which allows for a correction due to the finite-difference cell size (model cell is larger than the well diameter), introduces some error in the numerically simulated well water levels. For our application, the correction produces less drawdown at the well than would actually be expected during pumping with transient conditions. This is an inherent limitation with the synthetic water level dataset; thus a perfect fit to the numerically simulated values should not be expected.

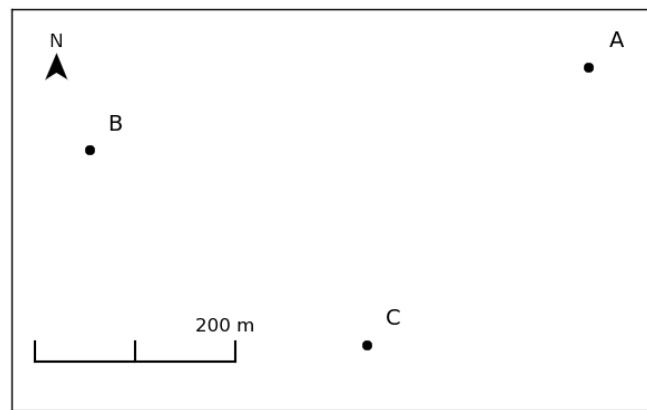


**Figure 13:** Synthetic well field map (plan view)

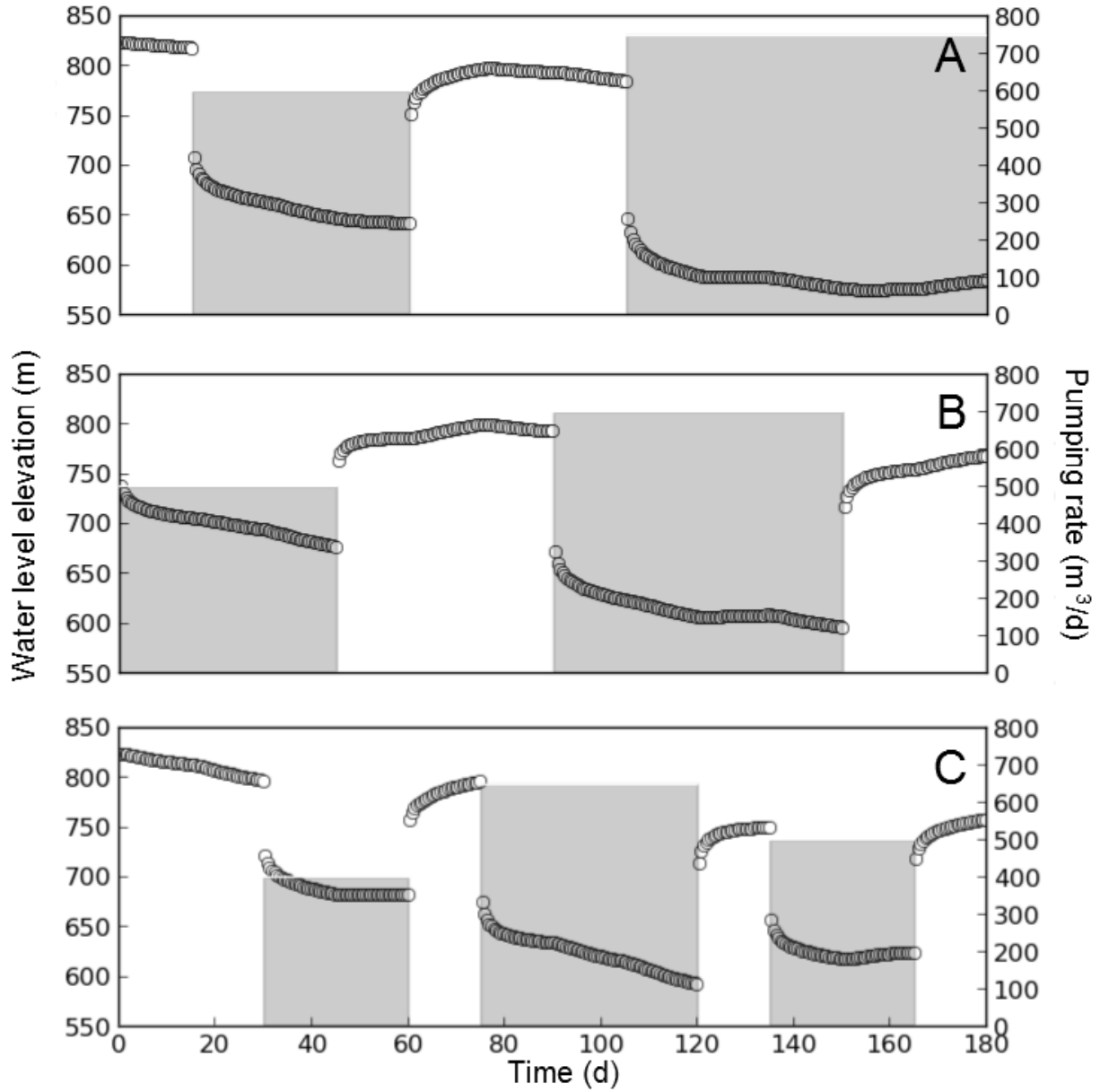


**Figure 14:** Simulated water levels (open circles) and modeled pumping rates (shaded bars) for synthetic well field.

#### 4.2.2 Results and Discussion

The model fit to our synthetic well field is shown in figure 15. An effective hydraulic conductivity was calculated using the estimated transmissivity and the thickness of our synthetic aquifer.

The best-fit effective hydraulic conductivity is shown in table 4 with the geometric and arithmetic mean hydraulic conductivities from our MPS model.

To investigate a potential bias in the estimated aquifer properties due to the finite-difference cell size correction, we performed a separate parameter estimation run where the objective function was formulated using only the earliest data from Well A (0-15 d) and Well C (0-30 d). During those time periods, pumping had not yet started at either well, so both locations can be regarded as observation points. Well A is 505 m (over 18 cell lengths) and Well C is 338 m (over 12 cell lengths) from the active Well B. Therefore the influence of the cell size correction is not expected to be significant at either location. The results of this second optimization run yielded nearly identical estimates of transmissivity ( $4.46 \text{ m}^2/\text{d}$ ) and storativity ( $5.43\text{e-}04$ ), indicating that the derivative behavior of the larger synthetic water level dataset is meaningful. Besides consideration of the cell size effect, this additional run provides support for our methodology in general (i.e., use of derivatives from our synthetic pumping wells gives a result that is similar to the more traditional analysis focused on observation well data).

The effective hydraulic conductivity was between the arithmetic and geometric mean hydraulic conductivities of our synthetic well field. For a heterogeneous field that follows a multivariate Gaussian distribution, the effective hydraulic conductivity converges to the geometric mean (Renard and de Marsily, 1997; Gomez-Hernandez and Wen, 1998; Wu et al., 2005). Our synthetic well field, which is generated by MPS does not necessarily have a distribution that can be as easily generalized. However, an effective  $K$  greater than the geometric mean is consistent with other studies that have considered groundwater flow in systems with channel deposits or other laterally continuous high- $K$  features (e.g., Zinn and Harvey, 2003; Ronayne and Gorelick, 2006).

Estimates of recoverable water level compared favorably to steady-state, pre-pumping water level elevations from our synthetic well field. The errors were all less than three meters and in one case was



less than one meter. Some error is expected from fitting a homogeneous to a heterogeneous model. Our estimates tended to all be high, which suggests a more systematic error due to the cell size correction.

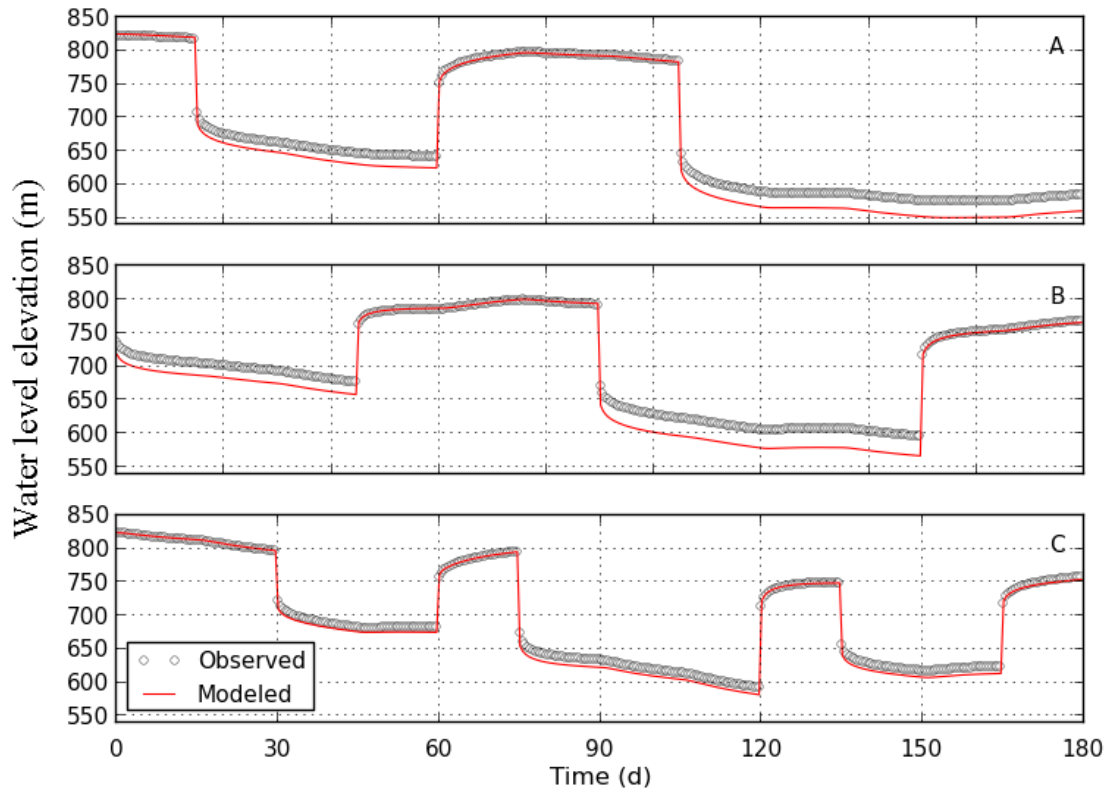


**Figure 15:** Fit of analytical model to synthetic water level observations after parameter estimation. Synthetic water level observations were generated using MODFLOW with the MNW2 package.

**Table 3:** Estimated aquifer properties for synthetic test cases. Synthetic model storativity was  $5.5 \times 10^{-4}$

Water level data used in objective function	Storativity ( $10^{-4}$ )	Transmissivity ( $\text{m}^2/\text{d}$ )
All Data	5.254	4.435
Observation Data Only	5.428	4.459

**Table 4:** Comparison of the effective hydraulic conductivity (obtained by parameter estimation) to mean K values for the entire heterogeneous field.

	<b>Hydraulic Conductivity (m/d)</b>
Parameter Estimation	0.040
Arithmetic Mean (synthetic)	0.052
Geometric Mean (synthetic)	0.022

**Table 5:** Comparison of the estimated recoverable water levels to synthetic water levels simulated for each well in the steady-state period prior to pumping.

<b>Well</b>	<b>Recoverable Water Level (m) (Synthetic)</b>	<b>Recoverable Water Level (m) (Model Fit)</b>
A	822.47	824.7
B	824.20	826.5
C	823.35	823.9

## CONCLUSIONS AND FUTURE RESEARCH DIRECTIONS

### 5.1 Summary and Conclusions

This thesis describes a new parameter estimation method to infer transmissivity and storativity from transient water levels measured at groundwater production wells. The method utilizes drawdown derivatives to estimate T and S. Analytically modeled drawdown derivatives are compared to derivatives estimated directly from the observed water level data. An optimization technique is used to identify best-fitting T and S values that minimize model residuals across the entire well field. Consideration of the derivative (slope) behavior initially eliminates uncertainty associated with recoverable water levels and well loss coefficients. The method was applied to real datasets from municipal well fields operating in the Denver Basin, and the estimated properties were shown to be consistent with values published elsewhere. Also considered was a synthetic water level dataset generated using a numerical model that incorporated the style of heterogeneity that occurs within the Denver Basin sandstone aquifers. Reasonable aquifer properties were identified for the synthetic model; the effective hydraulic conductivity (best-fit transmissivity divided by the modeled aquifer thickness) was slightly higher than the geometric mean hydraulic conductivity of the heterogeneous field.

After obtaining estimates of transmissivity and storativity in the parameter estimation workflow, subsequent optimization steps are used to identify the recoverable water level (modeled using a drift line) and well-loss coefficient for each groundwater production well. The effects of the drift line and well-loss coefficient estimates are related, and are therefore difficult to interpret in physical terms, but offer reasonable estimates of where to expect water levels in a production well to be.

Municipal well fields are typically not managed by professional groundwater modelers and operational constraints limit the types of pumping schemes that can be executed in practice. Our forward

model and parameter estimation method offers a simple way to assist in planning energy-saving, cost-effective pumping schedules at municipal well fields under local operational constraints. A model that can predict where well water levels are going to be under different pumping routines is a prerequisite to calculate the costs associated with pumping.

Data analysis is complicated by long-term effects, unknown parameters, and the necessity of considering aquifer and well mechanics simultaneously. However, automated data acquisition provides a very rich dataset to work with.

## **5.2 Future Research**

If the well loss functions in equations (3.3) and (3.4) are retained in future models, the model used for aquifer drawdown can be replaced by a different model. The Theis solution did not fully capture aquifer drawdown in our Arapahoe model; the leaky Hantush-Jacob solution [Hantush and Jacob, 1955], for example, may have provided better results. In other regions, one might use an unconfined analytical solution or even a numerical model. Our estimated aquifer properties may provide a useful starting guess for more complicated numerical analysis using tomography [Yeh and Liu, 2000; Zhu and Yeh, 2005], which may in turn be helpful in distinguishing the effects of heterogeneity from well-loss.

The computer code developed for this project analyze hourly time-series data to reduce the number of measured water levels and establish temporal discretization (periods of time with constant pumping rates) for the forward analytical model. This task relies on some initial processing of raw data from an automated data collection system to create a structured input file. Faster accessibility to data would make future analysis less time-consuming. Records should be automatically fetched and parsed from their original format into a more user-friendly format. A small future project might be development of a program that retrieves and performs this format conversion automatically.

Planning cost-effective pumping schedules that minimize energy expenditure is a difficult task due to operational constraints and unforeseen circumstances (e.g., a power outage). The reality is that

while a computer can generate innumerable possible pumping combinations, only a small subset can be executed in practice. A practical optimization method might involve rules of thumb and a simple interface whereby multiple practical pumping schedules could be tested quickly by an operator and planning done months in advance.

## REFERENCES

- [1] Anderman, G.G. and E.J. Ackman (1963), Structure of the Denver-Julesberg Basin and surrounding areas: Rocky Mountain Association of Geologists *Geol. Of the northern Denver Basin and adjacent uplifts*, p. 170-175.
- [2] Beckie, R., and C.F. Harvey (2002), What does a slug test measure: an investigation of instrument response and the effects of heterogeneity, *Water Resour. Res.*, 38(12), 1-14.
- [3] Bourdet, D., J.A. Ayoub, and Y.M. Pirard (1989), Use of pressure derivative in well-test interpretation, *SPE Form. Eval.*, 4(2), 293-302.
- [4] Comunian, A., P. Renard, and J. Straubhaar (2012), 3D multiple-point statistics simulation using 2D training images, *Computers & Geosci.*, 40, 49-65.
- [5] Cooley, R.L. (1985), A comparison of several methods of solving nonlinear regression groundwater flow problems *Water Resour. Res.*, 21(10), 1525-1538.
- [6] Jacob, C.E. (1947), Drawdown test to determine effective radius of artesian well, *Trans. Am. Soc. Civil Eng.*, 112, 1047-1070.
- [7] Crifasi, R.R. (1992), Alluvial architecture of the Laramide orogenic sediments: Denver Basin, Colorado, *The Mountain Geol.*, 29, 19-27.
- [8] Davis, J. (2013), Coupled analytical modeling of water level dynamics and energy use for operational well fields in the Denver Basin aquifers, M.S. Thesis, Colorado State University, Fort Collins, CO.
- [9] Domenico, P.A. and F.W. Schwartz (1990), Physical and Chemical Hydrogeology, John Wiley & Sons, New York, 824 p.
- [10] Gomez-Hernandez, J.J., and X.H. Wen (1998), To be or not to be multi-Gaussian? A reflection on stochastic hydrogeology, *Adv. Water Resour.*, 21, 47-61.
- [11] Hantush, M.S. and C.E. Jacob (1955), Non-steady radial flow in an infinite leaky aquifer, *Am. Geophys. Union Trans.*, 36(1), 95-100.
- [12] Harp, D.R., and V.V. Vesselinov (2011), Identification of pumping influences in long-term water level fluctuations, *Ground Water*, 49, 403-414.
- [13] Konikow, L.F., Hornberger, G.Z., Halford, K.J., and R.T. Hanson (2009), Revised multi-node well (MNW2) package for MODFLOW ground-water flow model: U.S. Geological Survey Techniques and Methods 6–A30.
- [14] Leven, C., and P. Dietrich (2006), What information can we get from pumping tests?-comparing pumping test configurations using sensitivity coefficients, *J. Hydrology*, 319, 199-215.
- [15] Marquardt, D. (1963), An algorithm for least-squares estimation of nonlinear parameters, *Journal of the Society for Industrial and Applied Mathematics*, 11, 431-441.

- [16] Meier, P.M., Carrera, J., and X. Sánchez-Vila (1999), A numerical study on the relationship between transmissivity and specific capacity in heterogeneous aquifers, *Groundwater* 37(4), 611-617.
- [17] Mutschler, F.E., Larson, E.E., and R.M. Bruce (1987), Laramide and younger magnetism in Colorado – New petrologic and tectonic variations on old themes, *Colorado School of Mines Quarterly*, 87, 1-47.
- [18] Obradovich, J.D. (2002), Geochronology of Laramide synorogenic strata in the Denver Basin, Colorado, *Rocky Mountain Geol.*, 37(2), 165-171.
- [19] Oliver, D.S. (1993), The influence of nonuniform transmissivity and storativity on drawdown, *Water Resour. Res.*, 29(1), 169-178.
- [20] Paschke, S.S. ed. (2011), Groundwater availability of the Denver Basin aquifer system, Colorado: U.S. Geological Survey Professional Paper 1770, 274 p.
- [21] Ramey, H.J. (1982). Well-loss function and the skin effect: A review, Recent trends in hydrogeology, *Geol. Soc. Am.*, special paper 189, 265-271.
- [22] Raynolds, R.G. (2002), Upper Cretaceous and tertiary stratigraphy of the Denver Basin, Colorado, *Rocky Mountain Geol.*, 37(2), 111-134.
- [23] Renard, P., Glenz, D., and M. Mejias (2009), Understanding diagnostic plots for well-test interpretation, *Hydrogeology J.*, 17, 589-600.
- [24] Renard, P., and G. de Marsily (1997), Calculating equivalent permeability: a review, *Adv. Water Resour.*, 20, 253-278.
- [25] Robson, S.G. (1987), Bedrock aquifers in the Denver Basin, Colorado – A quantitative water-resources appraisal: U.S. Geological Survey Professional Paper 1257, 73 p
- [26] Romero, J.C. (1976), Ground-water resources of the bedrock aquifers of the Denver Basin: Colorado Division of Water Resources Report, 109 p.
- [27] Ronayne, M.J., and S.M. Gorelick (2006), Effective permeability of porous media containing branching channel networks, *Phys. Review E*, 73, 026305.
- [28] Ronayne M.J., Gorelick, S.M., and J. Caers (2008), Identifying discrete geologic structures that produce anomalous hydraulic response: an inverse modeling approach. *Water Resour. Res.*, 44(8), W08426.
- [29] Rorabaugh, M.I. (1953), Graphical and theoretical analysis of step-drawdown test of artesian well, *Transactions, American Society of Civil Engineers*, 79, 362:1-23.
- [30] Sale, T., A. Bailey, and A. Maurer (2010), Studies supporting sustainable use of the Denver Basin aquifers in the vicinity of Castle Rock. Colorado State University Report. Project Report for the Town of Castle Rock.
- [31] Sánchez-Vila, X., A. Guadagnini, and J. Carrera (2006), Representative hydraulic conductivities in saturated groundwater flow, *Reviews of Geophys.*, 44, 1-46.

- [32] Soister, P.E., and R.H. Tschudy (1978), Eocene rocks in the Denver Basin, in Pruit, H.D., and Coffin, P.E., eds., *Energy resources in the Denver Basin: Denver, Rocky Mountain Association of Geologists Symposium*, 231-235.
- [33] Sterrett, R. J. (2007), *Groundwater and Wells*, 3rd Edition. New Brighton, Minnesota: Johnson Screens.
- [34] Straubhaar, J., Renard, P., Mariethoz, G., Froidevaux, R., and O. Besson (2011), An improved parallel multiple-point algorithm using a list approach. *Math Geosc.* 43(3), 305-328.
- [35] Theis, C. (1935), The relation between the lowering of the piezometric surface and the rate and duration of discharge of a well using ground-water storage, *Eos, Transactions, American Geophys. Union*, 16, 519-524.
- [36] Tumlinson, L.G., Osiensky, J.L., and J.P. Fairley (2006), Numerical evaluation of pumping well transmissivity estimates in laterally heterogeneous formations, *Hydrogeology Journal*, 14, 21-30.
- [37] Wu, C.-M., Yeh, T.-C. J., Zhu, J., Lee, T.H., Hsu, N.-S., Chen, C.-H., and A.F. Sancho (2005), Traditional analysis of aquifer tests: Comparing apples to oranges?, *Water Resour. Res.*, 41, W09402, doi:10.1029/2004WR003717.
- [38] Yeh, T.-C. J., and S. Liu (2000), Hydraulic tomography: Development of a new aquifer test method, *Water Resour. Res.*, 36(8), 2095-2105.
- [39] Zhu, J., and T.-C. J. Yeh (2005), Characterization of aquifer heterogeneity using transient hydraulic tomography, *Water Resour. Res.*, 41, W07028, doi:10.1029/2004WR003790.
- [40] Zinn, B., and C.F. Harvey (2003), When good statistical models of aquifer heterogeneity go bad: A comparison of flow, dispersion, and mass transfer in connected and multivariate Gaussian hydraulic conductivity fields, *Water Resour. Res.*, 39, 1051-1070.



## APPENDIX A

### INVERSE SOLUTIONS FOR ALL WELL FIELDS

#### A.1 Summary of Estimated Aquifer Properties at All Locations

Location	Storativity	Transmissivity (m <sup>2</sup> /d)	Transmissivity (gal/ft·d)
Arapahoe Aquifer			
Meadows	$2.0 \times 10^{-4}$	46.5	3740
Castle Oaks	$2.2 \times 10^{-4}$	35.8	2880
Founders	$2.4 \times 10^{-4}$	50.3	4050
Denver Aquifer			
Meadows	$2.0 \times 10^{-4}$	38.8	3120
Castle Oaks	$4.7 \times 10^{-4}$	30.0	2420
Founders	$9.4 \times 10^{-4}$	27.1	2180
Dawson Aquifer			
Meadows	$4.0 \times 10^{-4}$	10.6	850

#### A.2 Drift Lines

Note: drift line intercepts are at  $t_0$  occur on November 30, 2007

##### A.2.1 Arapahoe

	Well	$t_0$ Intercept (m)	Slope (m/yr)	$t_0$ Intercept (ft)	Slope (ft/yr)
Meadows	CR27	1516	-4.5	4973	-14.8
	CR28R	1518	-3.0	4980	-9.8
	CR49	1513	-0.8	4963	-2.6
	CR67	1557	-6.6	5108	-21.7
	CR82	1522	0.2	4993	0.7
	CR83	1532	-2.7	5026	-8.9
	CR86	1549	-2.9	5082	-9.5
	CR176	1547	-0.8	5075	-2.6
	CR219	1531	-3.6	5022	-11.8
	CR220	1517	-2.2	4977	-7.2
	CR223	1533	-3.4	5029	-11.2
Castle Oaks	CR73	1557	-3.7	5108	-12.1
	CR117	1563	-4.4	5127	-14.4
	CR118	1577	-0.5	5173	-1.6
	CR123	1584	-2.7	5196	-8.9
	CR124	1606	-6.6	5269	-21.7
Founders	CR31	1570	0.8	5151	2.6
	CR39	1550	3.7	5085	12.1
	CR43	1595	-5.8	5232	-19.0
	CR218	1578	-4.4	5177	-14.4

### A.2.1 Denver

	Well	$t_0$ Intercept (m)	Slope (m/yr)	$t_0$ Intercept (ft)	Slope (ft/yr)
Meadows	CR47	1656	-4.1	5433	-13.5
	CR50R	1652	-3.3	5420	-10.9
	CR51A	1680	0.4	5512	1.3
	CR84	1635	-3.8	5364	-12.5
	CR148	1648	-2.2	5407	-7.2
	CR149	1623	-0.2	5325	-0.7
	CR150	1656	-4.1	5433	-13.5
	CR174	1658	0.3	5440	1.0
	CR221	1643	-2.4	5390	-7.9
	CR224	1636	-3.3	5367	-10.8
Castle Oaks	CR72R	1736	-1.3	5696	-4.3
	CR101	1846	-8.8	6056	-28.9
	CR105	1786	-1.5	5860	-4.9
	CR110	1779	2.0	5837	6.6
	CR111	1779	-3.2	5837	-10.5
Founders	CR33R	1772	4.4	5814	14.4
	CR41	1802	-1.1	5912	-3.6
	CR45	1745	-2.6	5725	-8.5
	CR217	1792	-0.6	5879	-2.0

### A.2.1 Dawson

	Well	$t_0$ Intercept (m)	Slope (m/yr)	$t_0$ Intercept (ft)	Slope (ft/yr)
Meadows	CR152	1820	-0.5	5971	-1.6
	CR168	1818	-0.6	5965	-2.0
	CR170	1820	-6.4	5971	-21.0
	CR222	1810	0.6	5938	2.0
	CR225	1816	-1.0	5958	-3.3

### A.3 Well-Loss Coefficients

#### A.3.1 Arapahoe

	Well	Well-Loss Coefficient (d <sup>2</sup> /m <sup>5</sup> )	Well-Loss Coefficient (d <sup>2</sup> /ft <sup>5</sup> )
Meadows	CR27	0	0
	CR28R	0	0
	CR49	0	0
	CR67	0	0
	CR82	$2.6 \times 10^{-6}$	$6.8 \times 10^{-9}$
	CR83	$1.9 \times 10^{-5}$	$5.0 \times 10^{-8}$
	CR86	$1.0 \times 10^{-4}$	$2.6 \times 10^{-7}$
	CR176	0	0
	CR219	0	0
	CR220	0	0
	CR223	$7.7 \times 10^{-7}$	$2.0 \times 10^{-9}$
Castle Oaks	CR73	0	0
	CR117	0	0
	CR118	0	0
	CR123	$7.1 \times 10^{-7}$	$1.9 \times 10^{-9}$
	CR124	0	0
Founders	CR31	$2.2 \times 10^{-6}$	$5.8 \times 10^{-9}$
	CR39	0	0
	CR43	0	0
	CR218	0	0

(Page break inserted to make tables more readable)

### A.3.1 Denver

	Well	Well-Loss Coefficient (d <sup>2</sup> /m <sup>5</sup> )	Well-Loss Coefficient (d <sup>2</sup> /ft <sup>5</sup> )
Meadows	CR47	$7.1 \times 10^{-5}$	$1.9 \times 10^{-7}$
	CR50R	$2.8 \times 10^{-5}$	$7.4 \times 10^{-8}$
	CR51A	-	-
	CR84	$2.3 \times 10^{-5}$	$6.1 \times 10^{-8}$
	CR148	$2.9 \times 10^{-5}$	$7.6 \times 10^{-8}$
	CR149	0	0
	CR150	$1.6 \times 10^{-5}$	$4.2 \times 10^{-8}$
	CR174	$1.7 \times 10^{-5}$	$4.5 \times 10^{-8}$
	CR221	$8.6 \times 10^{-5}$	$2.3 \times 10^{-7}$
	CR224	$2.2 \times 10^{-6}$	$5.8 \times 10^{-9}$
Castle Oaks	CR72R	$2.5 \times 10^{-5}$	$6.6 \times 10^{-8}$
	CR101	$7.6 \times 10^{-5}$	$2.0 \times 10^{-7}$
	CR105	$6.8 \times 10^{-5}$	$1.8 \times 10^{-7}$
	CR110	$1.4 \times 10^{-5}$	$3.7 \times 10^{-8}$
	CR111	$1.2 \times 10^{-5}$	$3.2 \times 10^{-8}$
Founders	CR33R	$1.7 \times 10^{-5}$	$4.5 \times 10^{-8}$
	CR41	$3.1 \times 10^{-6}$	$8.2 \times 10^{-9}$
	CR45	$2.1 \times 10^{-5}$	$5.5 \times 10^{-8}$
	CR217	$7.2 \times 10^{-5}$	$1.9 \times 10^{-7}$

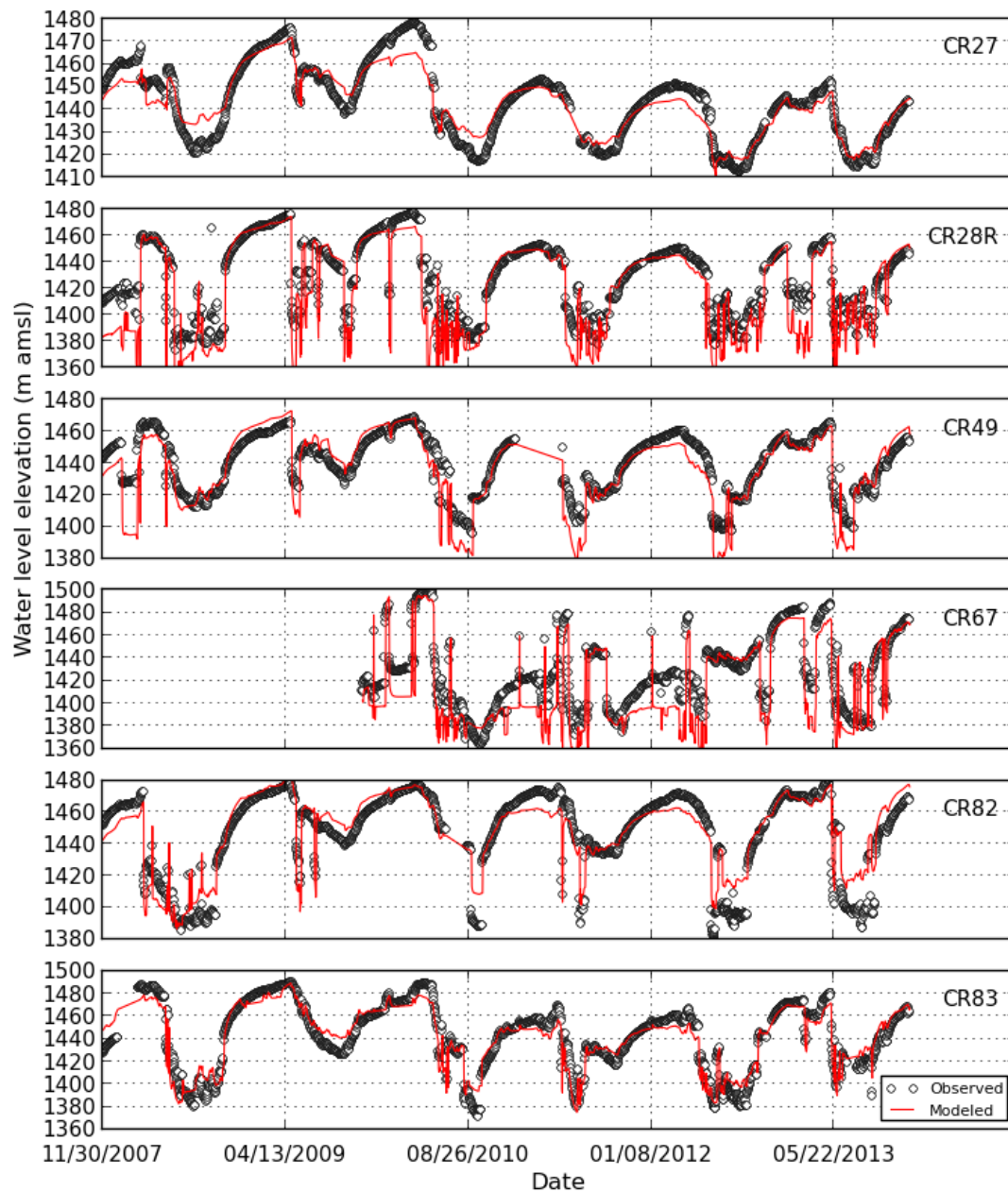
### A.3.1 Dawson

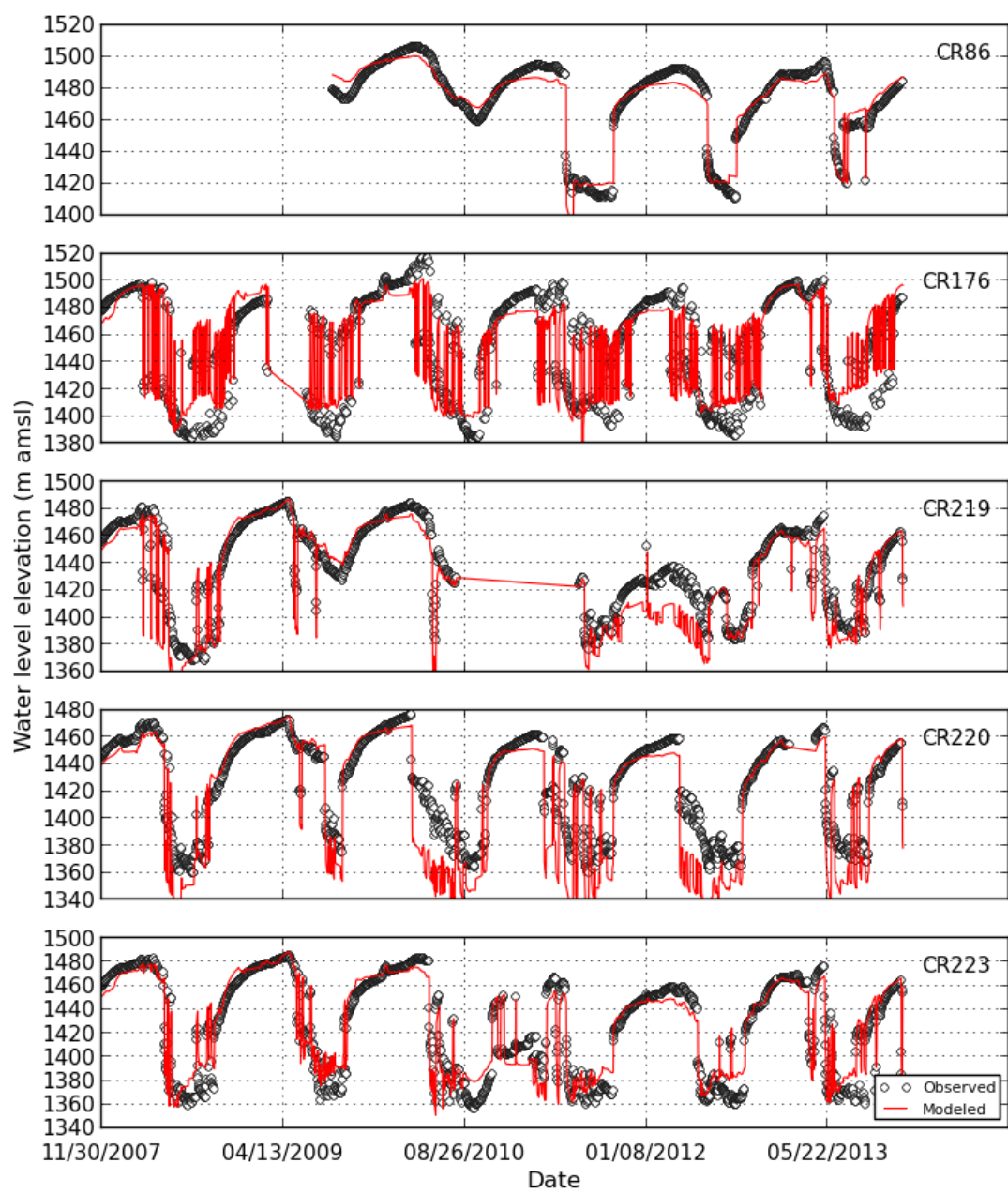
	Well	Well-Loss Coefficient (d <sup>2</sup> /m <sup>5</sup> )	Well-Loss Coefficient (d <sup>2</sup> /ft <sup>5</sup> )
Meadows	CR152	0	0
	CR168	0	0
	CR170	$1.9 \times 10^{-4}$	$5.1 \times 10^{-7}$
	CR222	$1.0 \times 10^{-5}$	$2.7 \times 10^{-8}$
	CR225	0	0

## A.4 Model Fit Hydrographs

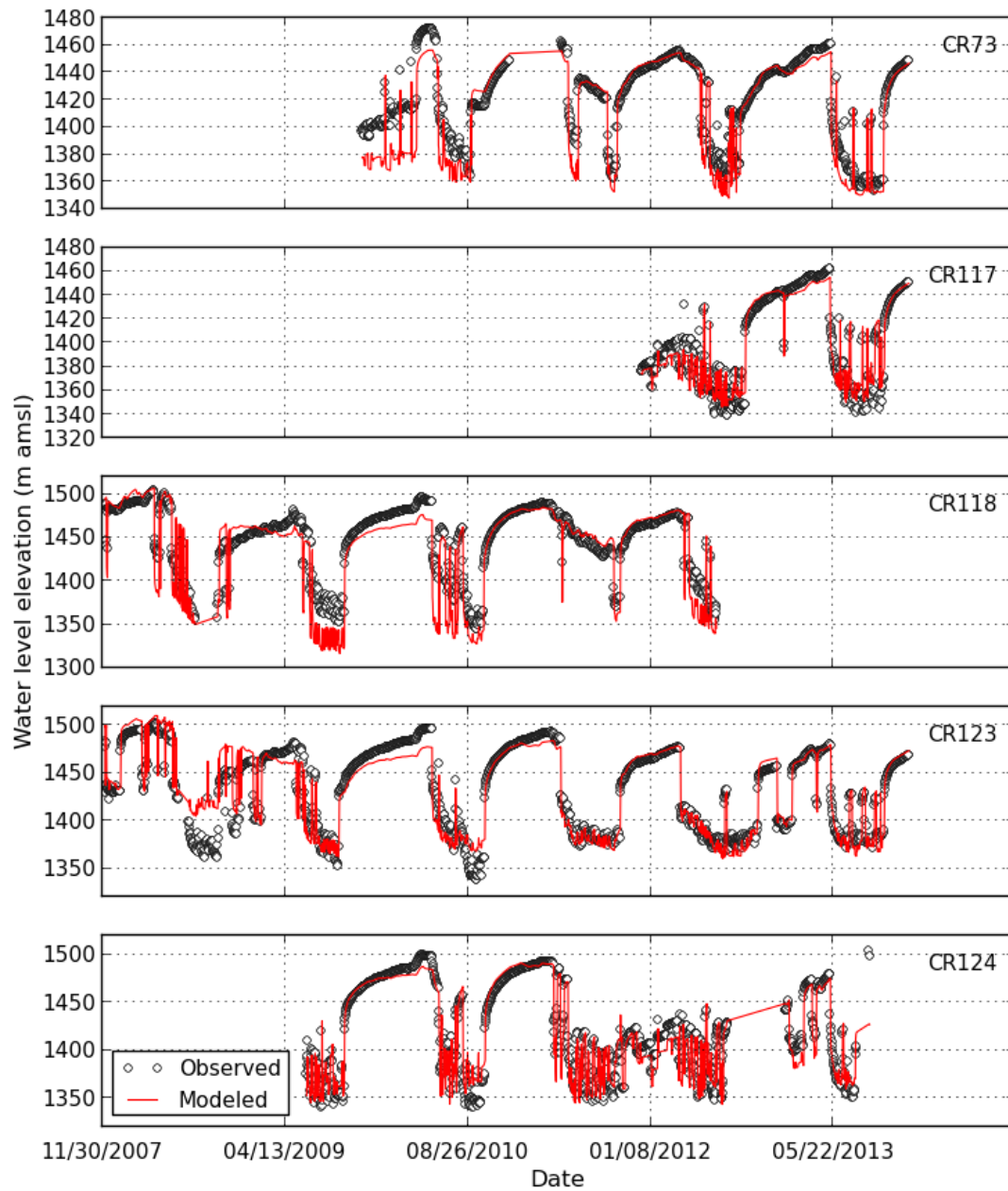
### A.4.1 Arapahoe

#### A.4.1.1 Meadows

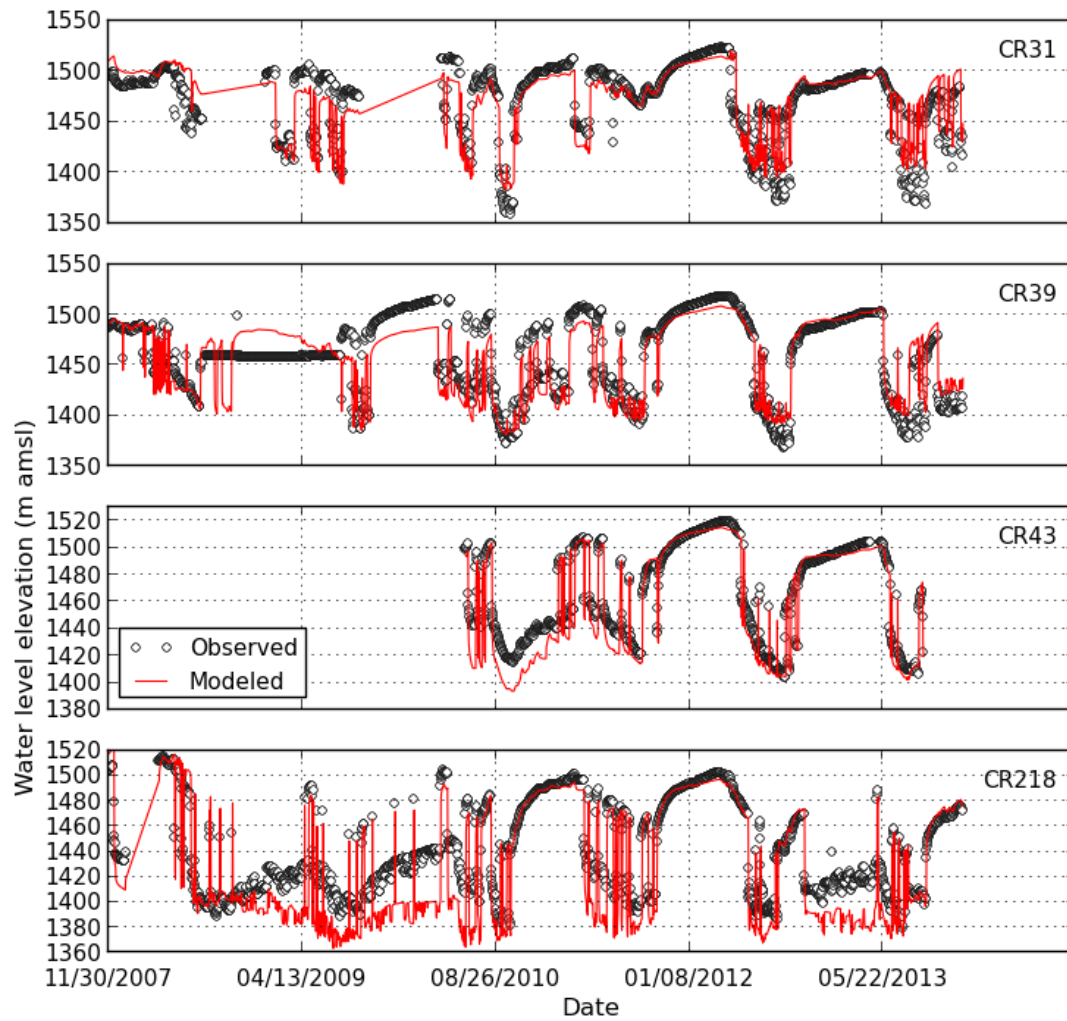




#### A.4.1.2 Castle Oaks



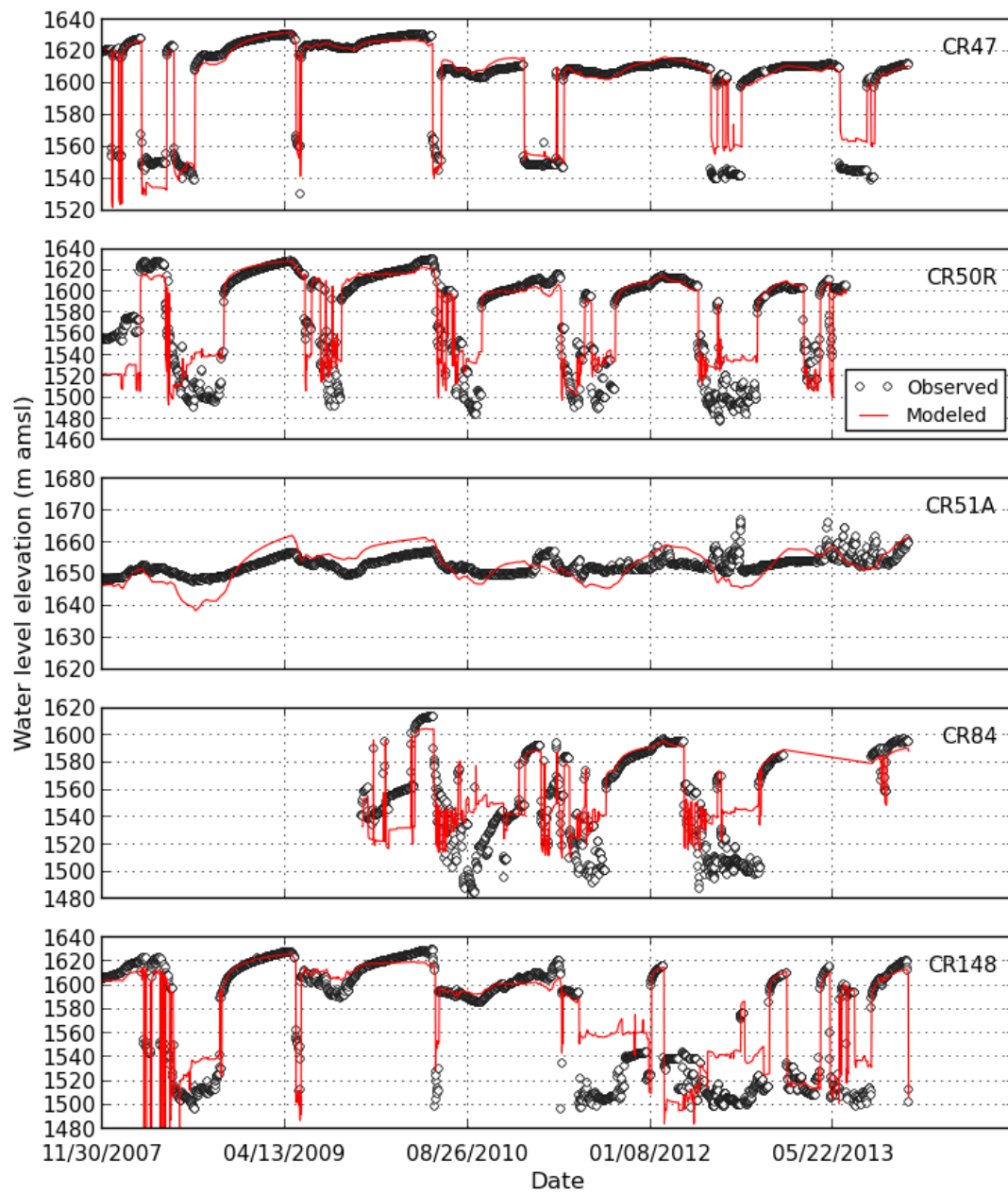
#### A.4.1.3 Founders

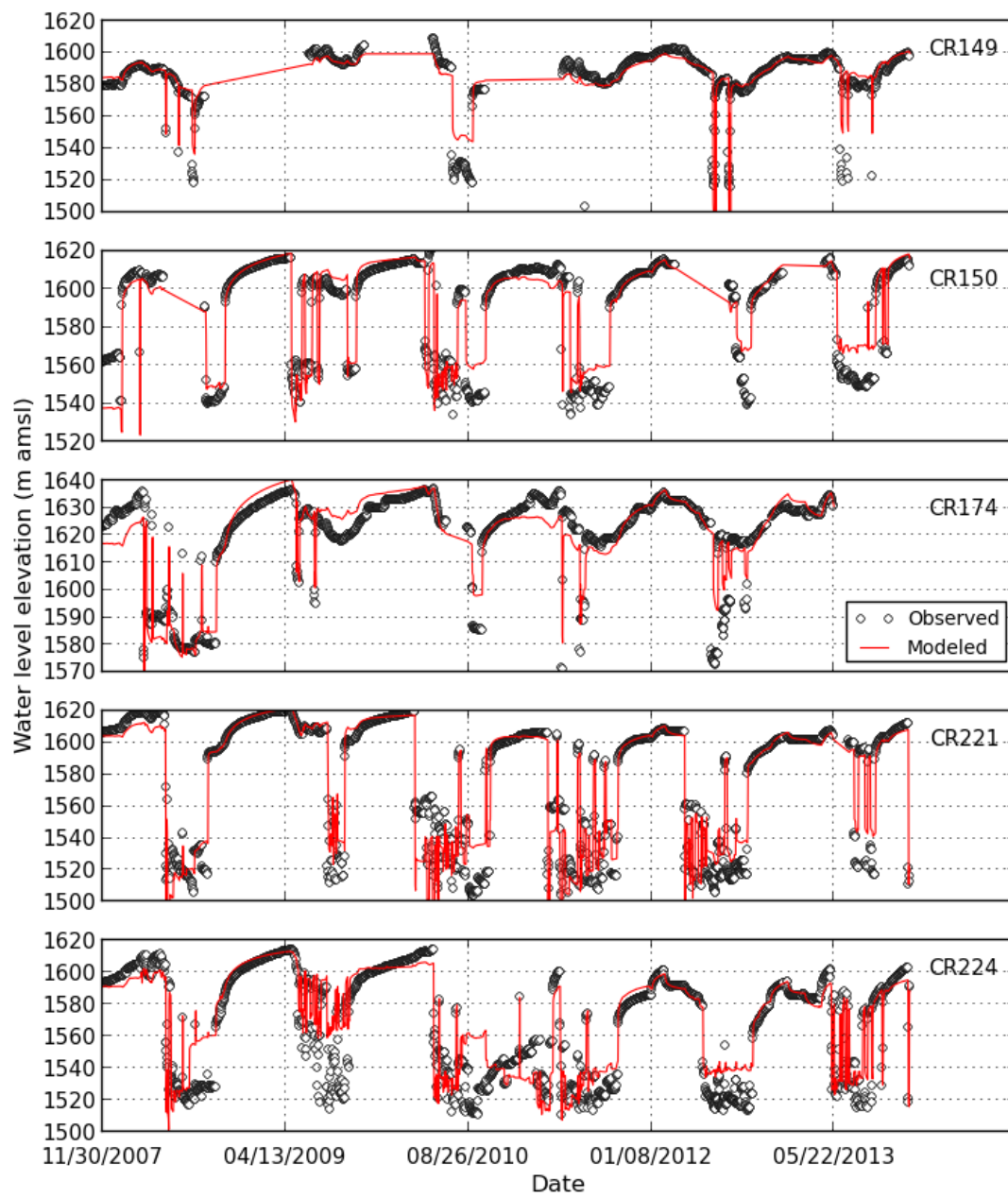




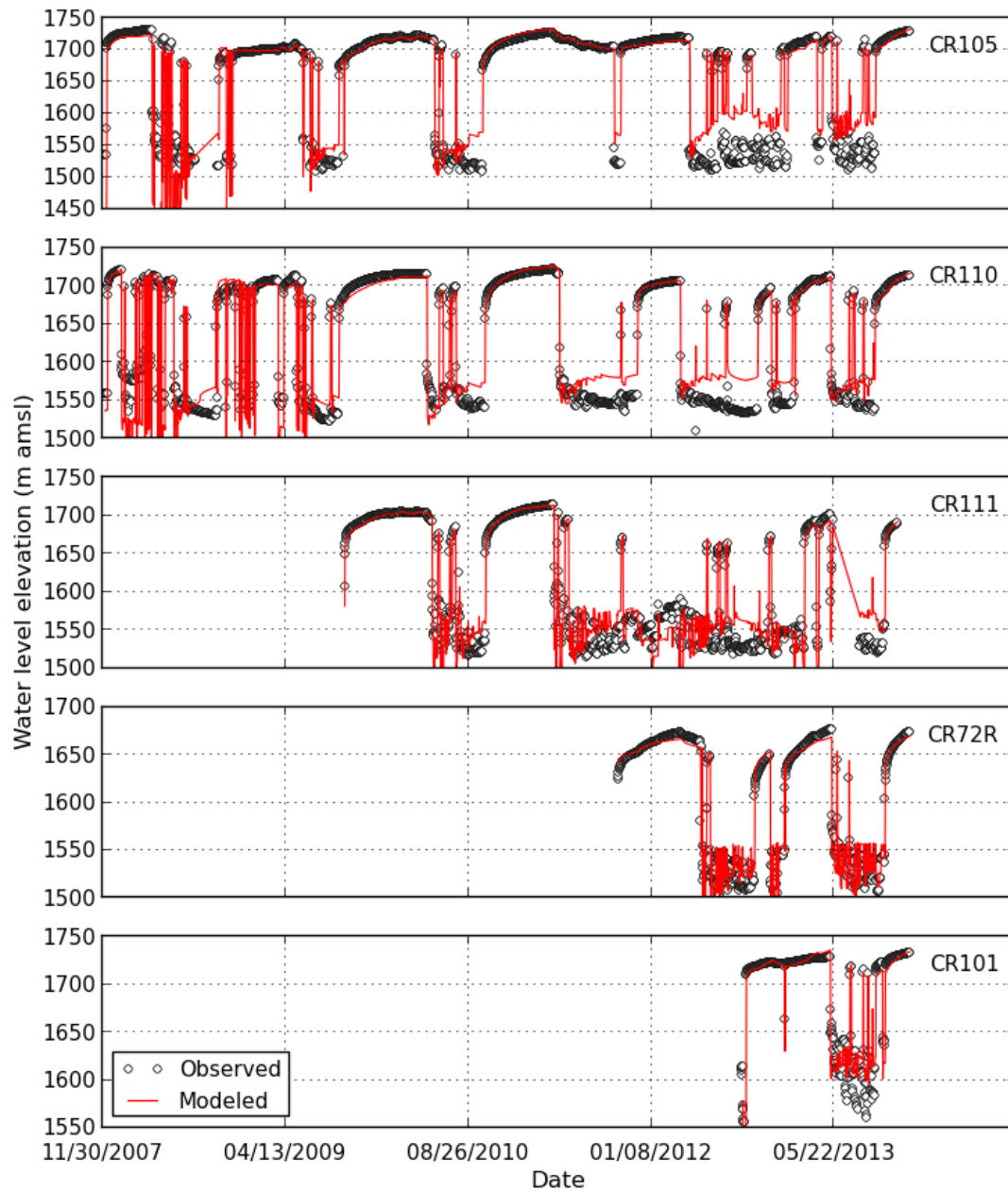
## A.4.2 Denver

### A.4.2.1 Meadows

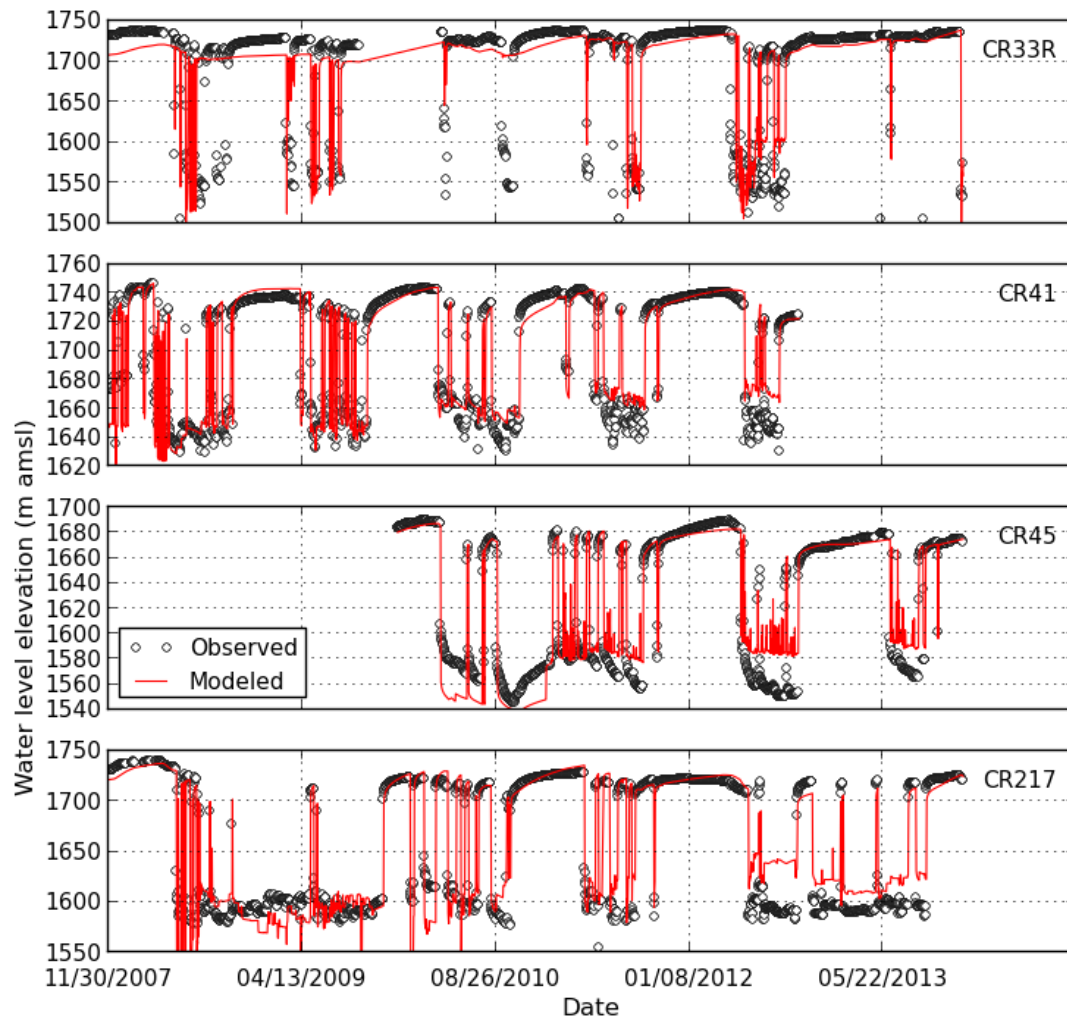




#### A.4.2.2 Castle Oaks

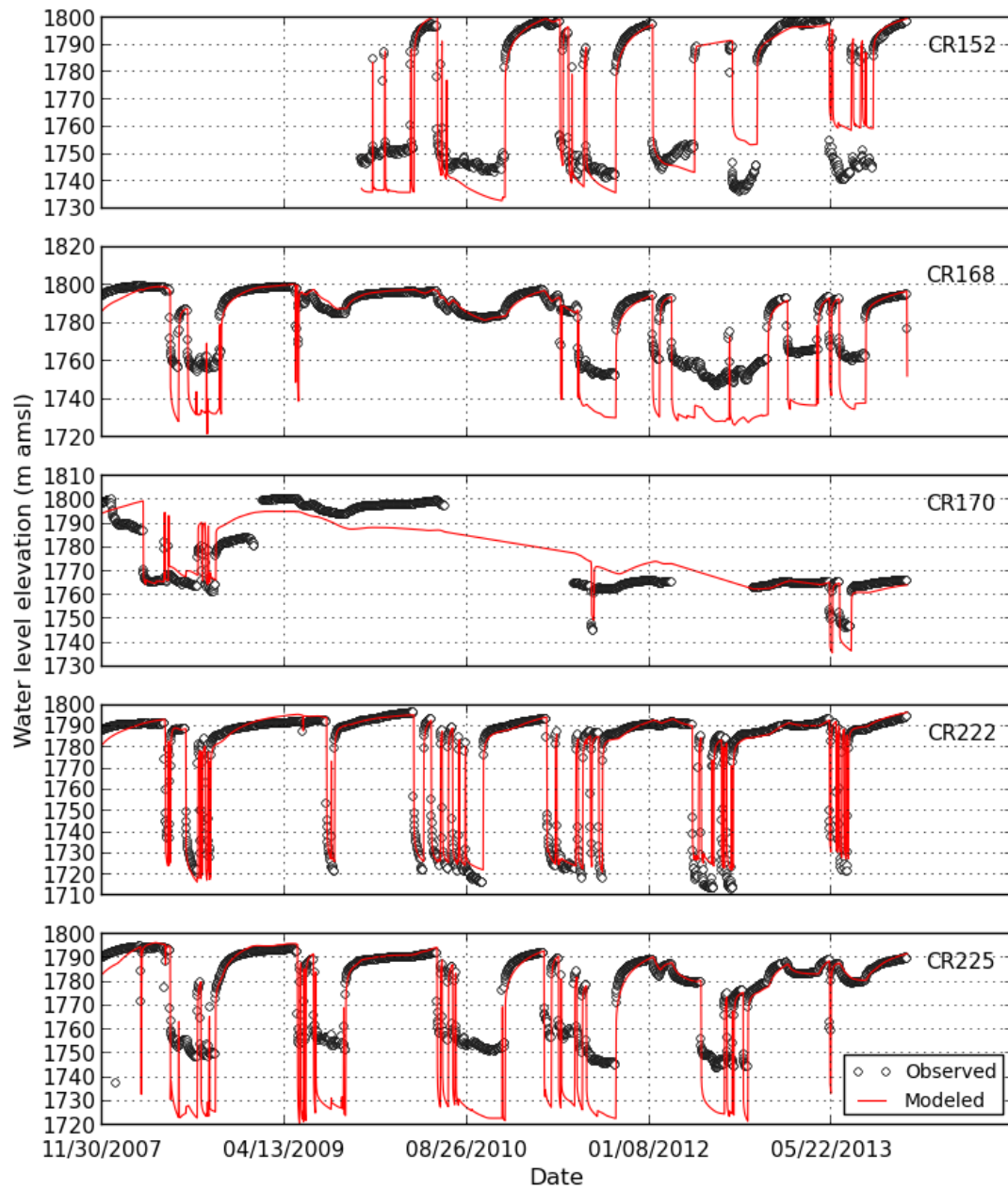


### A.4.2.3 Founders



### A.4.3 Dawson

#### A.4.3.1 Meadows



## APPENDIX B

### PYTHEIS INSTALLATION AND USAGE

The forward model and parameter estimator discussed in Chapter 3 were written in Python and C. All of the software is in a single package named PyTheis. This appendix provides instructions for the installation and application of PyTheis. For cases where inputs already exists in a structured database, it may be simpler to modify the core logic in *pytheis.py* to suit your needs.

#### B.1 Software Requirements (Installation Required)

Since PyTheis is written in Python, it does not require to be installed in the same sense most other programs are. A Python script is nothing more than a text document with a \*.py extension that is interpreted and executed by a Python interpreter. Python 2.x is required to run the scripts for this project.

Despite Python being a very feature-rich language, it does not come pre-packaged with all the tools necessary for the modeling and visualization applications presented in this thesis. Additional libraries for special functions, inverse solvers, and generating graphics also need to be installed. All dependencies are described below. There is some flexibility in which version one chooses for the dependencies and they are available pre-packaged in various ways. PyTheis was developed using the following dependencies: python-2.7.5.msi, numpy-1.7.1-win32-superpack-python2.7.exe, scipy-0.12.0-win32-superpack-python2.7.exe, matplotlib-1.2.1.win32-py2.7.exe, sip-4.14.7.zip, PyQt4-4.10.2.gpl.Qt4.8.4-x32.exe

##### B.1.1 Python Interpreter

At the time of writing this documentation, Python 3.x is the latest available version. Version 3.x broke backwards compatibility and some libraries used for this program have not yet completely shifted over from 2.x. Consequently, Python 2.x is required to run these scripts.

### **B.1.2 NumPy, SciPy, and Matplotlib**

NumPy is a package that adds array functionality. Much of the data in PyTheis is stored as an array, including well level measurements, pump rates, and drawdown. The SciPy package contains special functions, including the exponential integral that appears in the well function in the Theis solution and an implementation of the Levenberg-Marquardt least squares solver, used to inversely solve for aquifer parameters. Matplotlib is a flexible plotting package capable of generating the 2D and surface plots used in PyTheis.

### **B.1.3 PyQt**

PyQt is a Python wrapper for the C++ Qt library, which is a multi-platform widget toolkit capable of generating modern-looking graphical interfaces for Windows, Gtk, and OS X desktops. Qt5 is the latest release of the Qt framework, but this project was started prior to the release of Qt5. Consequently, it is necessary to use a version of PyQt wrapped around the Qt4 framework. Installation of PyQt is necessary when using the graphical user interface that accompanies PyTheis.

### **B.1.4 Troubleshooting**

It is assumed that the Python interpreter was properly installed. A Python command line environment can be opened from Start → Programs → Python 2.7 → IDLE (Python GUI). To check that all third-party packages are installed properly try importing them at the prompt:

```
>>> import numpy
>>> import scipy
>>> import matplotlib
>>> import PyQt4
```

If any of these commands returns an error, the the dependency is either not installed on your system or is not in the Python 2.x PATH. It is often worthwhile to copy and paste error messages into a web search engine to quickly resolve any common problems.

## **B.2 Software Requirements (Pre-Packaged)**

The GSL, PyTheis C extensions, and FFMPEG are likely to be pre-compiled in the PyTheis zip file, in which case installation may not be required.

### **B.2.1 GNU Science Library**

The GNU Science Library (GSL) is an open-source math library written in C. The only function needed from the GSL is the exponential integral (well function) of the Theis solution. There is an exponential integral function packaged with SciPy, however GSL was used in order to keep portions of the code (forward model calculations) in C. The result is that NumPy arrays can be passed to compiled C functions to be processed rather than embedding them in Python loops. If the GSL is not linking properly, `pytheis_old.py` may be renamed as `pytheis.py` (to run all functions in pure Python), but the increase in runtime is on the order of about 5-10 times.

### **B.2.2 FFmpeg**

FFmpeg is an open-source, cross-platform tool used for audio/video editing. It is used to convert a series of frames into an animation.



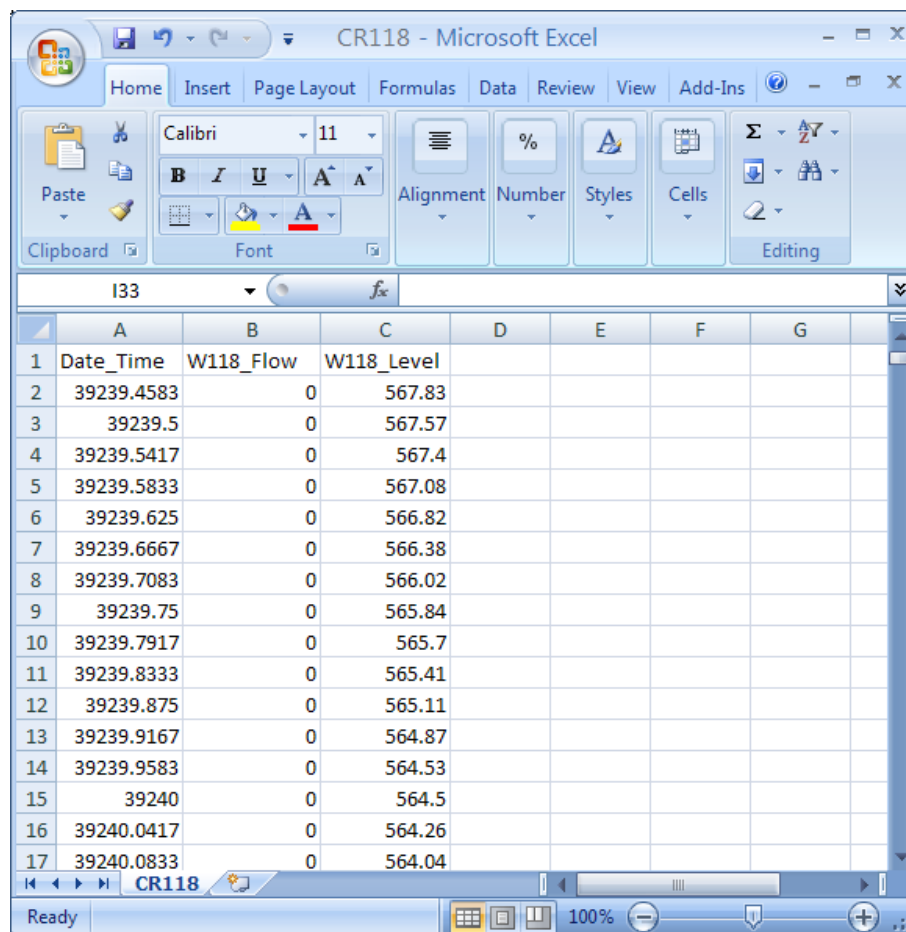
## B.3 GUI Usage

### B.3.1 Pre-Processing Data

PyTheis is designed to work with minimal pre-processing. Using a spreadsheet program,

1. Open a blank sheet
2. In row 1, label columns A, B, and C (in any way you choose)
3. Fill columns A, B, and C (in order) with time, pump rate, and water levels above probe.
4. Save as a .csv file in the *raw\_data/* folder of your Pytheis directory. You may create subdirectories, such that the full path of your .csv is something like:

*c:\pytheis\raw\_data\wellfield\_name\aquifer\_name\well01.csv*



The screenshot shows a Microsoft Excel window titled "CR118 - Microsoft Excel". The ribbon is set to "Home". The active cell is I33. The data is organized in a table with the following structure:

	A	B	C	D	E	F	G
1	Date_Time	W118_Flow	W118_Level				
2	39239.4583	0	567.83				
3	39239.5	0	567.57				
4	39239.5417	0	567.4				
5	39239.5833	0	567.08				
6	39239.625	0	566.82				
7	39239.6667	0	566.38				
8	39239.7083	0	566.02				
9	39239.75	0	565.84				
10	39239.7917	0	565.7				
11	39239.8333	0	565.41				
12	39239.875	0	565.11				
13	39239.9167	0	564.87				
14	39239.9583	0	564.53				
15	39240	0	564.5				
16	39240.0417	0	564.26				
17	39240.0833	0	564.04				

### B.3.2 Creating and Editing Wellfields

The screenshot shows the 'Wellfield Editor' window. It has a title bar with a question mark and a close button. The window is divided into two main sections. The top section, titled 'Inventory', contains three rows of controls. The first row is for 'Well Fields', with a dropdown menu showing 'castle oaks', an 'Add New' button, and a 'Remove' button. The second row is for 'Aquifer', with a dropdown menu showing 'denver', an 'Add New' button, and a 'Remove' button. The third row is for 'Well List', with a dropdown menu showing 'CR105', an 'Add New' button, and a 'Remove' button. The bottom section, titled 'Well Properties', contains several input fields. The 'Name' field is 'CR105'. The 'Radius (m)' field is '0.30'. The 'Easting (m)' field is '156825.39'. The 'Northing (m)' field is '1328848.10'. The 'Elevation (m)' field is '2011.68'. The 'Probe Depth (m)' field is '525.78'. The 'Relative Path' field is 'e\_oaks/denver/CR105.csv'. There is a 'Metric' checkbox which is checked. Below these fields is an 'Update Well Properties' button. At the bottom of the window are two buttons: 'Save Changes' and 'Close'.

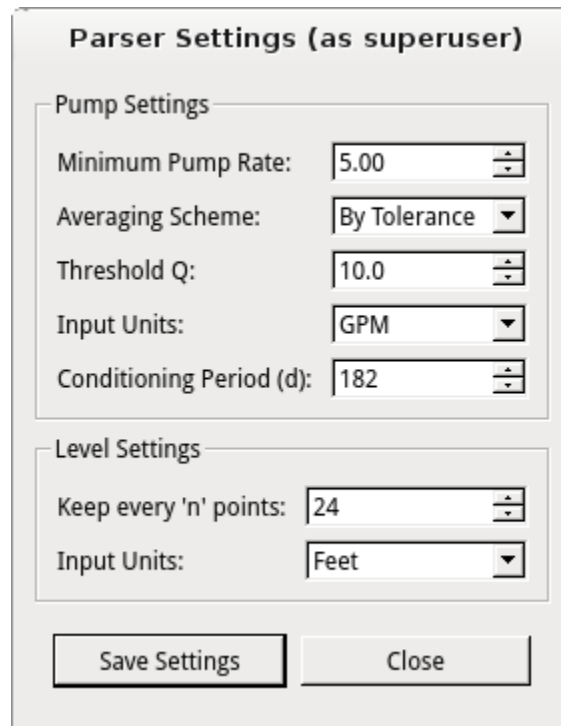
To launch the PyTheis well editing form, double-click on *wfedit\_dlg.pyw* from within the PyTheis directory. This will initially load well field properties that are specified in the example input file (*wells.json*), as shown in the above figure.

The relative path property of a well is the path to a pre-processed *.csv* file (as described in the previous section). Adding a new well defaults to a non-existent path called *path/to/file.csv*. This relative path would imply an absolute path of *c:\pytheis\raw\_data\path\to\file.csv*.

Changes to a set of well properties are temporarily changed when you click the “Update Well Properties” button. Changes are not written to the main input file until you click the “Save Changes” button.

The main input file is a JSON-formatted file called *wells.json*. Note that this file can be viewed in any text editor. Well properties may be edited in metric or imperial units, but they are always stored as metric.

### B.3.3 Setting Parsing Options



The image shows a dialog box titled "Parser Settings (as superuser)". It contains two sections: "Pump Settings" and "Level Settings".

**Pump Settings**

- Minimum Pump Rate: 5.00 (with up/down arrows)
- Averaging Scheme: By Tolerance (dropdown menu)
- Threshold Q: 10.0 (with up/down arrows)
- Input Units: GPM (dropdown menu)
- Conditioning Period (d): 182 (with up/down arrows)

**Level Settings**

- Keep every 'n' points: 24 (with up/down arrows)
- Input Units: Feet (dropdown menu)

At the bottom are two buttons: "Save Settings" and "Close".

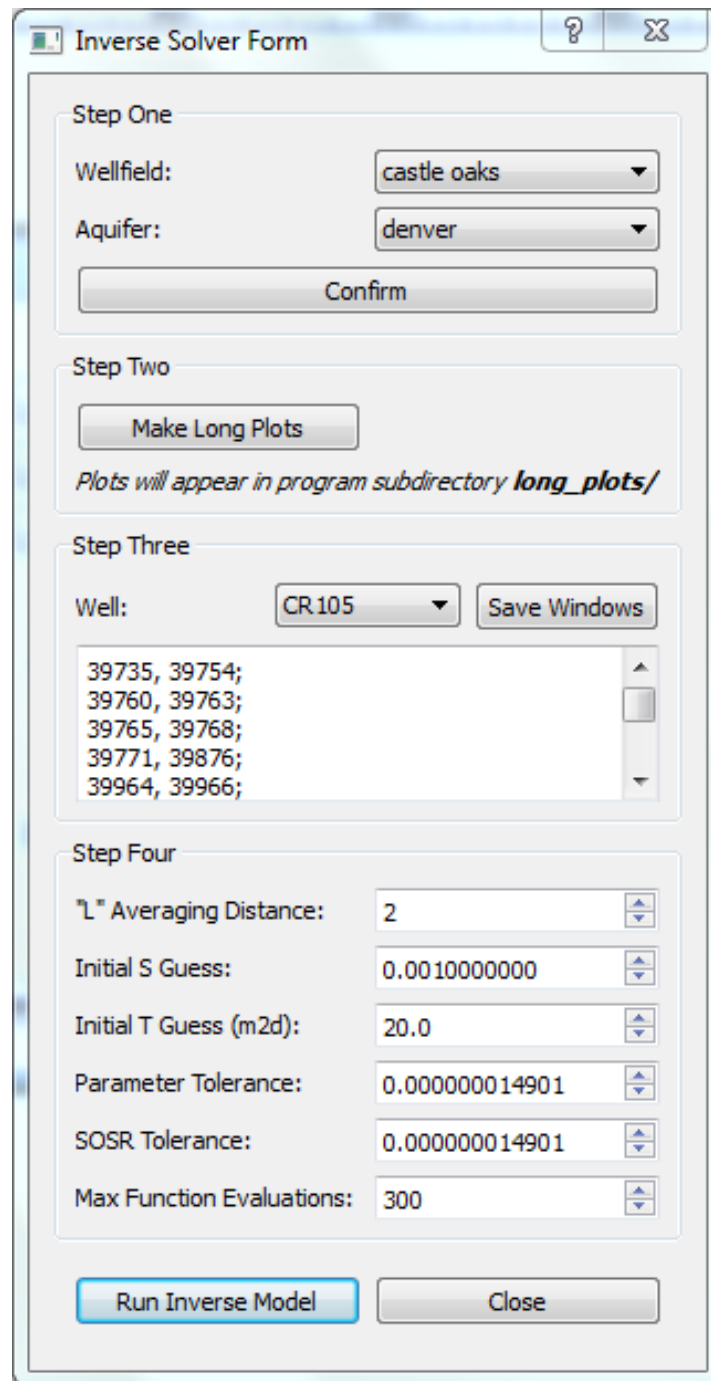
PyTheis contains a collection of functions for parsing raw data. These parsing functions take arguments that may be chosen by the user through the parser settings dialog (*parse\_dlg.pyw*). Available parser options include:

**Minimum Pump Rate** If set to  $Q_{min}$ , all pump rates  $Q$ , such that  $|Q| < Q_{min}$ , will be set equal to 0. In large well fields, small values like 5 gpm are negligible and may be ignored.

<b>Averaging Scheme</b>	If set to On/Off, the parser will average blocks of time when pumping is active. If set to “By Tolerance”, the parser will start a new block of time to average if the pump rate changes by more than “Threshold $Q$ ”
<b>Threshold <math>Q</math></b>	The change in pumping (or injection) that is required to establish a new block of time over which pump rates are averaged in the forward model.
<b>Input Units (flow rate)</b>	This should be consistent with the units for values in the second column of the CSV well input file.
<b>Conditioning Period</b>	The Theis solution assumes that the initial water level is equal everywhere (and known). In most real cases, the initial water level is not known, so it is a good practice to run the model for some time without fitting the predicted water levels to observed data. The conditioning period is how many days of pumping you would like to simulate before trying to fit observed levels. In cases where there are several years of data, 365 days may be a reasonable choice.
<b>Keep Every 'n' Points</b>	The trim interval is related to how sparsely you want to consider level readings. E.g., if 'trim interval' is set to 24, then only every 24th observed level will be simulated. This method does no averaging. It is simply removal of dense data.
<b>Input Units (level)</b>	This should be consistent with the units for values in the third column of the CSV well input file.

When the “Saved Changes” button is clicked, parser settings will be saved to the file *parse\_settings.py*.

### B.3.4 Conducting Parameter Estimation



The image shows a software dialog box titled "Inverse Solver Form". It is divided into four steps for configuring an inverse model.

**Step One**

Wellfield:

Aquifer:

**Step Two**

*Plots will appear in program subdirectory **long\_plots/***

**Step Three**

Well:

**Step Four**

"L" Averaging Distance:

Initial S Guess:

Initial T Guess (m2d):

Parameter Tolerance:

SOSR Tolerance:

Max Function Evaluations:

The parameter estimation form is an interface for estimating storativity and transmissivity in an aquifer using the Levenberg-Marquardt algorithm.

The parameter estimation form may be launched by running *inverse\_dlg.py*. A console will also be launched to display values at each step of the inverse procedure. The input for parameter estimation is specified using four steps:

### **Step One: Select Wellfield and Aquifer**

Use the combo boxes to select the wellfield and aquifer for which you would like to estimate parameters for. Click the “Confirm” button.

### **Step Two: Make Long Plots**

A "long" plot is an individual well hydrograph that illustrates water level versus time for the entire period of record. In PyTheis, the "long" plots are used to identify temporal windows with high-quality data where meaningful drawdown derivatives can be calculated.

Click the “Make Long Plots” button. After a few seconds, a series of plots will be generated in a PyTheis subdirectory called *long\_plots/*. You are likely going to need to zoom in to view them properly.

### **Step Three: Select Windows to Fit**

A “window” in PyTheis is defined as a period of time over which observed level readings are considered. The long plots created in step two will help identify appropriate windows.

For the parameter estimation to work properly, windows of time which overlap with changes in pump rates must not be considered. In the long plots, vertical blue lines indicate when a pump was switched off and red lines indicate when a pump was either switched on or when a change in pump rate occurred. Select windows such that they do not contain any blue or red lines.

The inverse solver relies on fitting the numerical derivative of observed levels over time to a modeled derivative. Observed derivatives are very sensitive to noise, so it is best to select windows with smooth behavior.

To add windows, select a well, and then enter the time range using the following format (using a new line for each window):

$$t_0, t_f;$$

#### **Step Four: Select Parameters for Inverse Solver**

Step four requires selection of parameters required by the inverse solver. They are:

**"L" Averaging  
Distance**

The observed derivative is smoothed by averaging a derivative with neighboring points. L is a value (in days) over which a derivative is calculated. Note: if your data contains any windows with gaps (time intervals between measurements) larger than L days, the program will likely crash.

**Initial S Guess**

The initial storativity value given to the solver.

**Initial T Guess**

The initial transmissivity value given to the solver in units of m<sup>2</sup>/d

**Parameter Tolerance**

The parameter tolerance is the value by which successive iterations of the LM algorithm must improve estimates of S and T. If consecutive iterations do not improve S or T by the parameter tolerance, the LM will finish.

**SOSR Tolerance**

The inverse solver minimizes the sum-of-squared residuals between observed and modeled data. If the difference in SOSR between successive iterations is less than this tolerance (negligible improvement) convergence is reached and the solver will stop. The tolerance is set to a default value and may not need to be changed depending on the amount of observed data and the anticipated magnitude of the residuals.

**Max Function Evaluations**

This is how many iterations the inverse solver is given to find a solution. It is set to a default value that probably does not need to be changed.

**B.3.4 Run Inverse Model**

Click "Start Param Estimation" button. Each iteration will be printed to the console that was launched with your parameter estimation form. Final results will be presented as plots in the relative path *inverse\_model/*.

**B.3.5 Creating an Animation**

The animaton form may be launched by opening *animation\_dlg.py*.

**xmin, xmax, ymin, ymax**

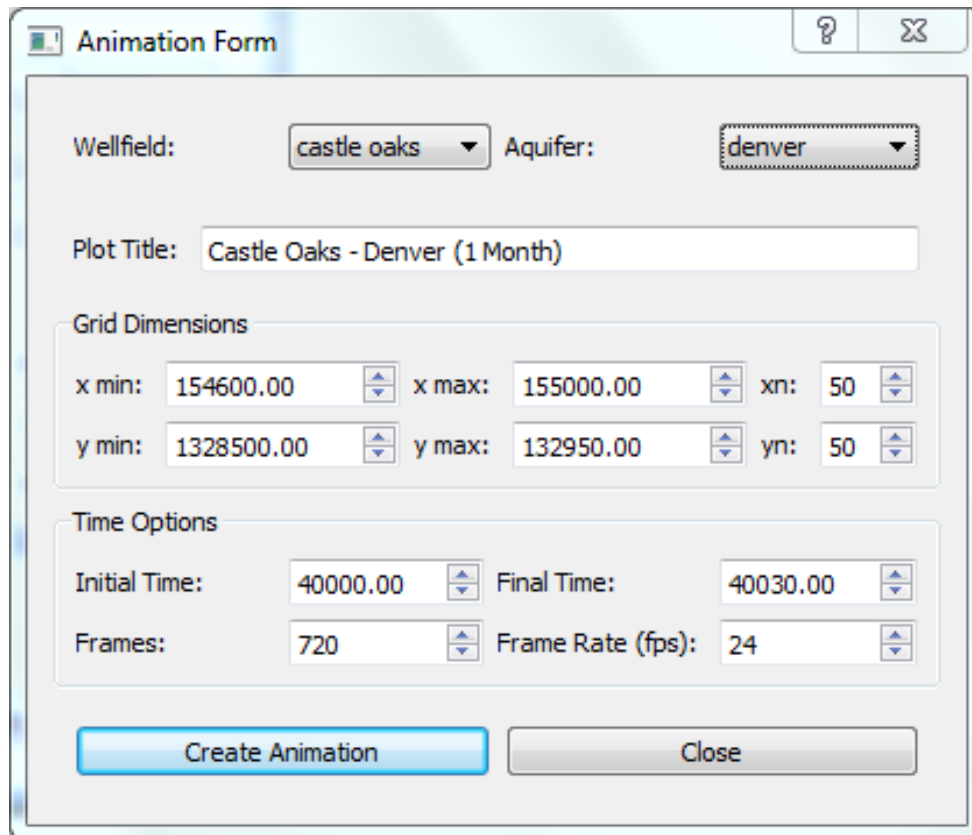
Easting (x) and northing (y) boundaries expressed in meters.

**xn, yn**

How finely to discretize the surface grid. E.g., a value of 50 for xn will create 50 grid points in the east-west direction



**Initial and Final Time** The start and end time for the animation in days. If you're using dates imported from Excel, time is given in days since Jan-0, 1990. Check your original .csv file for a good interval.



The screenshot shows a software window titled "Animation Form". It contains several input fields and buttons. At the top right are icons for help (?) and close (X). The "Wellfield:" dropdown is set to "castle oaks" and the "Aquifer:" dropdown is set to "denver". The "Plot Title:" text field contains "Castle Oaks - Denver (1 Month)". Below this is a "Grid Dimensions" section with fields for "x min:" (154600.00), "x max:" (155000.00), "xn:" (50), "y min:" (1328500.00), "y max:" (132950.00), and "yn:" (50). Each of these fields has small up/down arrow buttons. Below the grid dimensions is a "Time Options" section with fields for "Initial Time:" (40000.00), "Final Time:" (40030.00), "Frames:" (720), and "Frame Rate (fps):" (24). Each of these fields also has up/down arrow buttons. At the bottom are two buttons: "Create Animation" (highlighted in blue) and "Close".

Frames for animation will be placed in Pytheis subdirectory *frames/*, where they will need to be manually deleted between each animation. The final animation will be in the Pytheis main directory and given the filename *output.mp4*. If your computer does not have the necessary codecs to play this format, we recommend VLC media player, which may be downloaded at no cost.